arXiv:astro-ph/0611931v3 20 Dec 2006

TRANSITIVE X-RAY SPECTRUM AND PeV GAMMA-RAY CUTOFF IN THE M87 JET: ELECTRON "PEVATRON"

Mitsuru Honda

Plasma Astrophysics Laboratory, Institute for Global Science, Mie, Japan

Yasuko S. Honda

Department of Electrical and Information Engineering,
Kinki University Technical College, Mie, Japan;
yasuko@ktc.ac.jp

ABSTRACT

We propose a modified version of the X-ray spectral index and an intrinsic cutoff frequency of inverse Compton radiation from the brightest knot of the M87 jet, in conjunction with an application of the new conceptions of injection and diffusive shock acceleration (DSA) of electrons in magnetized filamentary plasma to the specified source. The drop of the X-ray flux density in a transitive frequency region is associated with the interplay of ordinary synchrotron cooling and weaker magnetic fields concomitant with the smaller scale filaments that allow the electron injection, while the radio-optical synchrotron continuum is dominantly established by the major electrons that are quasi-secularly bound to larger filaments. With reference to, particularly, the updated external Compton model, we demonstrate that in the Klein-Nishina regime fading inverse Comptonization, the injected electrons can be stochastically energized up to a Lorentz factor as high as 5×10^{10} in the temporal competition with diffuse synchrotron cooling; this value is larger than that attainable for a simple DSA scenario based on the resonant scattering diffusion of the gyrating electrons bound to a supposed magnetic field homogeneously pervading the entire knot. The upper limits of the photon frequency boosted via conceivable inverse Compton processes are predicted to be of the common order of $\sim 10^{30}$ Hz. The variability of the broadband spectrum is also discussed in comparison to the features of a blazar light curve. The present scenario of a peta-eV (PeV; 10^{15} eV) electron accelerator, the "Pevatron," might provide some guidance for exploring untrod hard X-ray and gamma-ray bands in forthcoming observations.

Subject headings: acceleration of particles — galaxies: individual (M87) — galaxies: jets — gamma rays: theory — magnetic fields — radiation mechanisms: nonthermal

1. INTRODUCTION

A fundamental question — the observable highest frequency of radiation from extragalactic jets — remains unresolved, as the closely relevant physics of the particle acceleration incorporated with injection and the cosmological transport of energetic photons is largely unknown in both theoretical and observational aspects. As a candidate celestial object to study those issues in detail, of a suitable nature is a nearby powerful radio source, particularly the M87 jet, and so far, many efforts have been devoted to measure the photon spectra in higher frequency bands (optical, Meisenheimer et al. 1996; Perlman et al. 2001; X-ray, Marshall et al. 2002; Wilson & Yang 2002). In the previous key work that was based on ground-based observations (Meisenheimer et al. 1996), the synchrotron spectra were suggested to, in the entire jet, have an almost constant cutoff of $(0.8 - 2.5) \times 10^{15}$ Hz (see also Pérez-Fournon et al. 1988; Stiavelli et al. 1997), compared to a universal value among radio jets (Keel 1988). The corresponding Lorentz factor of the electrons was estimated to be 9×10^5, which could be deduced from a simple model of the diffusive shock acceleration (DSA) that relied on the small-angle resonant scattering by the turbulent Alfvén waves (Biermann & Strittmatter 1987; Longair 1992). However, state-of-the-art *Chandra* observations revealed that the spectra indicate no steep cutoffs, extending to X-ray regions (Marshall et al. 2002), far beyond the previous cutoff. The X-ray continua have been ascribed to synchrotron radiation, whereas inverse Compton (IC) models as a dominant X-ray mechanism have been ruled out. The Lorentz factor of the X-ray–emitting electrons is considered to be of order $\sim 10^6 - 10^8$ (Meisenheimer et al. 1996; Perlman et al. 2001; Marshall et al. 2002; Wilson & Yang 2002), although the achievable maximum is as yet poorly known.

A clue to this puzzling question is that simple models invoking shocks and synchrotron losses in a uniformly filled jet overpredict the X-ray flux density by large factors (Biretta et al. 1991; Marshall et al. 2002). In fact, the fine structure of magnetized filaments including the limb-brightening feature has been found at many positions along the jet (Reid et al. 1989; Owen et al. 1989; Stiavelli et al. 1991; Lobanov et al. 2003). The cancellation of the small-scale magnetic fields could be responsible for the observational fact that in the interior of the jet, the magnetic field is significantly free (Owen et al. 1989), reducing the polarization (Capetti et al. 1997). Accordingly, the requirement for modeling a nonuniform jet is that in the interior the turbulent state ought to be rather vital, in contrast to conventional jet models involving a turbulent radial edge (e.g., Ostrowski 2000) caused by surface-mode instabilities such as the Kelvin-Helmholtz instability.

At this juncture, the novel model by Honda & Honda (2002), in which the jet is hypothesized to comprise the magnetized filaments that are self-organized via a current filamentation instability (Honda et al. 2000a), seems to satisfy this requirement. In their model, the vec-

tors of fluctuating magnetic fields in the interior are supposed to be randomly oriented in the transverse direction of the filaments, such that they could be macroscopically canceled out, although in the envelope region, the uncanceled, ordered magnetic field could appear (Honda & Honda 2004a, 2005a). By invoking a similar environment, Fleishman (2006) has recently examined synchrotron radiation from the electrons injected into the small-scale random magnetic fields and found that the diffuse emission including higher harmonics reproduced the observational X-ray continuum at the knots B and C1. However, the mechanisms of the electron injection reflecting the energy hierarchy that ought to be involved in the filamentary plasma (Honda & Honda 2005a) and the related in situ acceleration were not self-consistently taken into consideration. It is important to investigate these details, because the complex interplay will actually connect the confirmed radio-optical continuum with the diffuse synchrotron spectrum in the energetic regime to give a transitive spectrum compared to the observed X-ray spectrum (Marshall et al. 2002), which is expected to deviate from the conventional model spectrum simply involving the synchrotron cooling (e.g., Kardashev 1962; Longair 1994). Also, the injected electrons quickly lose the coherency of their trajectory in the filamentary (stochastic) medium and thereby have a shorter mean free path (mfp) that deviates from the universal gyroscaling (valid for the simple case in which a mean magnetic field can be well defined); this is just the case that is advantageous to the DSA. The possible reboost of electron energy will, in turn, upshift the IC gamma-ray cutoff frequency.

In the context of the filamentary jet model, here we propose a novel scheme to construct the steepened X-ray synchrotron spectrum (§ 2) and attempt to provide genuine uppermost energies of an accelerated electron and photon at knot A (§ 3), where X-ray flux is so prominent as to be comparable to that from the galactic core (Marshall et al. 2002; Perlman & Wilson 2005). The theory is based on the DSA model incorporated with the new type of injection reflecting electron escape from small-scale magnetic traps, which is referred to as the "transition injection" (§ 2.1). We obtain a modified X-ray spectral index consistent with the large flux density reduction measured in the *Chandra* regime and a nonlinearly evolving feature of the current filamentation instability (§ 2.2). In the conceivable radiation fields, including external Compton (EC) targets (Stawarz et al. 2003), we find that the injected electrons can be, in situ, accelerated up to the 10 PeV range (§ 3.1). It is shown that the flux density of IC radiation surpasses, above the soft gamma-ray region, that of synchrotron radiation, and the highest frequency reaches the theoretical upper limit reflecting the maximum electron energy (§ 3.2). The IC spectrum can be accommodated with the recent High Energy Stereoscopic System (HESS) observation of sub-TeV gamma rays emanating from the galaxy region (Beilicke et al. 2005), although the origin of these gamma rays is still unresolved. The energy budget of the diffuse synchrotron radiation in

the gamma-ray spectral tail is also estimated (§ 3.3). Moreover, we include a discussion concerning the variability of the broadband spectrum (§ 4). The presence of fine filaments turns out to be essential for the transition injection, raising the flux density level of the diffuse radiation and engendering the high-frequency variation, and therefore the observability of such filaments is also discussed (§ 5).

2. SYNCHROTRON SPECTRUM EXTENDING TO THE X-RAY BAND WITHOUT STEEP CUTOFF

Highlighting the conception of the transition injection that mediates the energy hierarchy involved in a magnetized filamentary plasma, we consider the electron preacceleration below the injection energy. First we recover the radio-optical synchrotron continuum in the cold limit (§ 2.1), and second, we construct the transitive X-ray spectrum (§ 2.2).

2.1. *Impacts of the Small Spatioscale Entailed in the Transition Injection*

Begin by considering a low-energy state in which cosmic-ray (test) electrons are bound to the magnetized current filaments with various transverse sizes λ, exhibiting gyromotion. Apparently, this can be compared to the low-β plasma state, and along with this, it seems to be reasonable to suppose that the locally ordered fields, with a strength of $|\mathbf{B}(\mathbf{r})|$, permeating through the filaments, are preferentially disturbed by Alfvén waves. As is accommodated by the test particle approximation, we presume a small-amplitude disturbance that does not affect the zeroth-order magnetic fields sustained by the bulk filaments (the validity is confirmed later). In this aspect, recalling the consensus that the jet knots are associated with shocks, the *gyrating* cold electrons can presumably be accelerated by a conventional Fermi-based DSA mechanism relying on the weak Alfvénic fluctuations. For a possible case of the scattering center compression ratio of $r \sim 4$ (reflecting a high Mach number shock; Vainio 1999; Schlickeiser 2002), the predicted synchrotron emission from the nonthermal electrons is certainly compatible with the observed radio-optical continuum of the power-law flux density distribution ($F_\nu \propto \nu^{-\alpha}$), which has indices around $\alpha \sim 0.5$ (Biretta et al. 1991); that is, assigning the α-value to the canonical expression $\alpha_1 = (p-1)/2$ (e.g., Longair 1994) gives a differential spectral index of the electron density of $p = (r+2)/(r-1) \sim 2$ (for $dn/d\epsilon = \kappa\epsilon^{-p}$, where $\epsilon = \gamma mc^2$). It is precisely noted that in general, the relation of r to the gas compression ratio depends on the plasma conditions, such as the plasma β-value (see Vainio 1999; Schlickeiser 2002, for the detailed calculations). As long as the gyroradius of the accelerated electrons $r_{g,e}$ is smaller than the transverse size of the local filament

trapping them ($\sim \lambda$), such a DSA mechanism will safely operate. With regard to energy restrictions, the acceleration of the electrons bound to a large filament ought to be knocked down by radiative losses before the escape from the filament (temporal limit), whereas the electrons bound to a small filament could escape via the energization (spatial limit). It is, thus, anticipated that there exists a critical scale of filament, λ_c, that discriminates between the large and small scales. Furthermore, with reference to the consequence of kinetic simulations that the amplification of magnetic fields accompanies the coalescence of filaments accumulating larger filaments (Honda et al. 2000a,b), we consider a situation in which the filaments with larger (smaller) values of λ involve the larger (smaller) values of $|\mathbf{B}|$. Here we invoke the scaling of $|\mathbf{B}| \propto \lambda^{(\beta-1)/2}$, where β corresponds to the power-law spectral index of the magnetized filamentary turbulence (possibly larger than the spectral index for the Kolmogorov turbulence; Montgomery & Liu 1979; Honda & Honda 2005a).

In order to quantitatively examine the λ dependence of the maximum Lorentz factor of an accelerated electron γ^*, of practical use is an extended scheme that can treat the oblique mean magnetic field with respect to the shock normal direction (for the methodological details, see Honda & Honda 2004b). We consider a simple model in which the energy density ratio of the fluctuating magnetic field to $|\mathbf{B}|^2/(8\pi)$, denoted as b ($\ll 1$), is spatially constant, and the scattering of electrons occurs when the wave-particle resonance condition of $r_{g,e} \sim k^{-1}$ is satisfied, where the wavenumber k is supposed to be in the inertial range of the power-law fluctuation spectrum with an index of β' (e.g., $\beta' = 5/3$ for the Kolmogorov-type fluctuations; Biermann & Strittmatter 1987; Honda & Honda 2004b). Note that the local minimum of k (i.e., the correlation length of the Alfvénic fluctuations) is compared to the filament size λ, whose maximum is described as $\tilde{l}D$, where $\tilde{l}$ ($\lesssim 1$) and D denote the reduction factor of the filament correlation length and the diameter of the jet, respectively (typically, $\tilde{l}D = 110$ pc is expected at knot A; Biretta et al. 1991).

As concerns the radiative losses of accelerated electrons, we take normal synchrotron and IC cooling into account. The former is ascribed to the gyration in the local mean field, whose intensity can be expressed in the phenomenological form of $|\mathbf{B}| = B_m(\lambda/\tilde{l}D)^{(\beta-1)/2}$, where $B_m \equiv |\mathbf{B}|_{\lambda=\tilde{l}D}$. The diffuse effects considered in § 3 are ignored because $b \ll 1$. For the latter, it should be remarked that while the synchrotron self-Compton (SSC) process can be preferentially ignored (§ 3.1), influential EC candidates do exist, including the starlight and extended dust emission of the host galaxy (Stawarz et al. 2003). At knot A, which is at a distance of 1 kpc from the galactic core (Honda & Honda 2004a), the energy densities of the target photons are, in the comoving (shock rest) frame, suggested to be of the levels of $u_{\rm ph} \sim 10^{-9}\Gamma^2$ ergs cm^{-3} (stars) and $\sim 10^{-11}\Gamma^2$ ergs cm^{-3} (dust), where $\Gamma = (1 - U^2/c^2)^{-1/2}$ is the Lorentz factor of the shock. The cosmic microwave background (CMB), which arranges $u_{\rm ph} \simeq 4 \times 10^{-13}\Gamma^2$ ergs cm^{-3}, plays a minor role in determining γ^*. These EC scatterers

would uniformly pervade at the concerned region, such that $u_{\rm ph}$ = const is assumed, in contrast to the inhomogeneous $|\mathbf{B}|$ (which is dependent on λ).

In Figure 1, for a dominant stellar emission level of $u_{\rm ph} = 10^{-9}$ ergs cm^{-3} and a promising parameter set of $\beta = 4.3$ (for the reasoning, see § 2.2), $\beta' = 5/3$, and $\tilde{l}D = 110$ pc, we show the λ dependence of γ^* for a fixed $b = 10^{-3}$, given $B_m = 100\ \mu$G $- 10$ mG as a parameter (*top*), and for $B_m = 1$ mG, given $b = 10^{-4} - 10^{-2}$ (*middle*). Here we have set the compression ratio to $r = 3.2$ (for $p \simeq 2.3$, inferred from the radio-optical index of $\alpha = 0.67$ at knot A; Perlman et al. 2001), the shock speed to $U = 0.5c$ (as compared to the pattern speeds at knot A; Biretta et al. 1995), and the inclination angle of the local mean field to the maximum: $\cos^{-1}(U/c) = 60^\circ$ (e.g., Owen et al. 1989; Capetti et al. 1997; Heinz & Begelman 1997). It is found that in any case, γ^* appears to take the peak value at a certain value of $\lambda = \lambda_c$, and as seen in Figure 1 (*top*), both $\gamma^*_c \equiv \gamma^*|_{\lambda=\lambda_c}$ and λ_c decrease as B_m increases. For the electrons bound to the small filaments with a size of $\lambda < \lambda_c$, the γ^* value is determined by the simple relation of $r_{g,e}(\propto \gamma^*/|\mathbf{B}|) \sim \lambda$ that yields $\gamma^* \propto \lambda^{(\beta+1)/2}$, while for the electrons bound to the large filament with $\lambda > \lambda_c$, a radiative loss limits the acceleration. For the former spatial limit, the γ^*-value is independent of b, as seen in Figure 1 (*middle*). As for the latter temporal limit, in general, the balance between the mean acceleration time, which has an approximate dependence of $\propto r_{g,e}(\lambda/r_{g,e})^{\beta'-1}$ (Honda & Honda 2004b), and either the synchrotron cooling time, $\propto (\gamma^*|\mathbf{B}|^2)^{-1}$ or the IC time, which has dependencies of $\propto (\gamma^*)^{-1}$ (in the Thomson limit) and $(\ln\gamma^*)^{-1}$ (in the high-energy limit of the Klein-Nishina regime), yields the scaling of the form of $\gamma^* \propto \lambda^{-\mu}$, where

$$\mu = \begin{cases} \mu_{\rm syn} = [(\beta+1)\,\beta' - 2] \,/\, [2\,(3-\beta')]\,, \\ \mu_{\rm T} = [(\beta+1)\,(\beta'-1) - (\beta-1)] \,/\, [2\,(3-\beta')]\,, \\ \mu_{\rm KN} \simeq \mu_{\rm T}[(3-\beta') \,/\, (2-\beta')], \end{cases} \tag{1}$$

respectively. In the displayed cases, the shortest loss time is that of the synchrotron cooling, such that the scaling with $\mu = \mu_{\rm syn} = 2.6$ appears, although for a less likely case in which both B_m and b are small, an IC limit with $\mu \sim \mu_{\rm KN} = 0.35$ can appear (not shown in the figure).

In Figure 1 (*bottom*), for the convincing parameters (at knot A) of $B_m = 4.59$ mG (equal to the upper limit suggested by Owen et al. 1989) and $b = 10^{-3}$ (see § 2.2), we explicitly show the discrimination between the spatial (*dotted line*) and temporal (*solid curve*) limits, indicating the DSA tracks for gyrating electrons trapped in the filament with $\lambda < \lambda_c = 1.7$ pc (*solid arrows*) and $\lambda > \lambda_c$ (*dotted arrows*). It is also demonstrated that in a high-energy regime and the possible frequency range of the target photon field (see § 3.1), the Klein-Nishina effects reduce the IC loss, fading the Thomson regime with $\mu_{\rm T} = 0.087$ (*thin dot-dashed line*); as a result, the synchrotron cooling solely contributes to determine γ^* for the

temporal limit regime, yielding a single scaling with $\mu_{\rm syn}$ (= 2.6, without μ-flip; *solid curve*). In any case, one can identify a critical Lorentz factor of $\gamma_c^* = 7.6 \times 10^9$ at which all minor electrons bound to the small filaments with $\lambda < \lambda_c$ can escape from them ("escape tracks") to spaciously meander in a forest of the magnetized filaments. For the escaping electrons, more efficient energization is anticipated, as explained in § 3.1, wherein the critical energy $\gamma_c^* mc^2$ is pertinently compared to the injection energy for the additional DSA. We note that the major electrons quasi-secularly bound to the large filaments with $\lambda > \lambda_c$ ("secular-trap tracks") cannot reach the critical level of γ_c^* because of the synchrotron cooling.

This type of injection associated with the escape from the gyrotraps (namely, the bound-free transition) has been referred to as the transition injection (Honda & Honda 2005a). It should be again noticed that the "escape" does *not* mean the leak of energetic electrons from the jet, but merely the escape from the magnetized fine filaments with $\lambda < \lambda_c$; that is, for the escape electrons to be additionally accelerated, of course, they still need to be confined in the shock accelerator. More details of the additional DSA are discussed in § 3.1.

2.2. *X-Ray Spectral Index Linked to Turbulent Spectral Indices*

In the low-energy regime below γ_c^*, the gyrating electrons bound to the filaments continuously emit polarized synchrotron photons in an ordinary fashion. Thus, for the conventional Fermi-based DSA that engenders the power-law electron distribution (denoted in § 2.1), the resulting flux density of synchrotron radiation conforms to the generic scaling $F_\nu \propto \kappa \nu^{-(p-1)/2} |\mathbf{B}|^{(p+1)/2}$ (Longair 1994). For simplicity, we set $\kappa =$ const at the moment. If we recall the scaling of $|\mathbf{B}| \propto \lambda^{(\beta-1)/2}$, then it follows that the most dominant contribution to F_ν comes from the electrons bound to the filaments with an outer scale of $\lambda \sim \tilde{l}D$. On the other hand, the familiar scaling of the synchrotron cutoff above which F_ν exponentially decays, $\nu^* \propto (\gamma^*)^2 |\mathbf{B}|$ $\nu^* \propto \gamma^{*2} |\mathbf{B}|$ (valid for $\gamma^* \gg 1$), is found to lead to $\nu^* \propto \lambda^{-[2\mu-(\beta-1)/2]}$ in the secular-trap tracks of $\lambda_c < \lambda \leq \tilde{l}D$ (cf. Fig. 1, *bottom*). Hence, for values of $\mu > (\beta-1)/4$, which are typical for $\mu = \mu_{\rm syn}(\beta' \neq 1)$, the F_ν spectrum includes the most dominant component having a lowermost ν^*, which is considered to dominantly contribute to establish the so-called "break frequency" (commonly identified in the optical to soft X-ray band; Perlman et al. 2001; Marshall et al. 2002). The property that the less dominant component involves a higher ν^* cooperates to steepen the F_ν spectrum, in accordance with the X-ray measurement that indicates that the F_ν level falls below that inferred from extrapolation of the featureless radio-optical continuum to the X-ray region. The F_ν drop in the frequency change from $\nu_b \equiv \nu^*|_{\lambda=\tilde{l}D}$ to $\nu_c^* \equiv \nu^*|_{\lambda=\lambda_c}$ can be estimated as

$$\phi = \Big[\lambda_c/(\tilde{l}D)\Big]^{(p+1)(\beta-1)/4} . \tag{2}$$

Note that equation (2) is, through λ_c, dependent on B_m and b (see Fig. 1, *top* and *middle*).[1]

In Figure 2, for $(\beta, \beta') = (4.3, 5/3)$, given $b = 10^{-4} - 10^{-2}$, we plot ν_b (*top*), ν_c^* (*middle*), and ϕ (*bottom*) as a function of B_m for the typical value of $\tilde{l}D = 110$ pc (*thick curves*) and a shorter value of $\tilde{l}D = 11$ pc (*thin curves*). The shock conditions have been chosen to be the same as those for Figure 1. It appears in Figure 2 (*top*) that ν_b decreases as B_m increases, according to the dependence of $\nu_b \propto B_m^{-[4\mu_{\rm syn}/(\beta-1)-1]} = B_m^{-2.1}$ in the regime in which the synchrotron cooling definitely limits the value of γ. In the major ranges of B_m and b, as seen in the middle panel, ν_c^* remains almost constant, since the change of $|\mathbf{B}|_{\lambda=\lambda_c}$ is canceled out by that of $(\gamma_c^*)^2$ in the synchrotron-limiting regime. Also, in the corresponding regime, along the dependence of $\phi \propto \lambda_c^{2.8}$, the decrease of λ_c with increasing B_m (Fig. 1, *top*) leads to the decrease of ϕ, as depicted in the bottom panel of Figure 2. Note that for a small value of B_m (leading to a small $|\mathbf{B}|_{\lambda=\lambda_c}$), the appearance of the synchrotron limit can be incomplete for a small b that lowers γ_c^* (Fig. 1, *middle*) to weaken the Klein-Nishina effect; this property yields the peculiar B_m dependencies of ν_c^* and ϕ in the marginal (B_m, b)-domain, as shown in the middle and bottom panels of Figure 2. The values of ν_b, ν_c^*, and ϕ are likely enhanced for large values of b, and, in addition, ν_b and ϕ are further boosted for the small value of $\tilde{l}D$, although ν_c^* is unchanged, except for the IC-limiting regime. With regard to a comparison with the observational data, for a confirmed radio-optical F_ν spectrum with index $\alpha = 0.67$ (Biretta et al. 1991; Perlman et al. 2001), for example, a value of $\nu_b \simeq 7 \times 10^{14}$ Hz is expected for a common X-ray spectrum (of the core and the brightest knots, including knot A) consistent with a simple power law with $\alpha = 1.46 \pm 0.05$ (Marshall et al. 2002; for alternative, see below). For the case of $\tilde{l}D = 110$ pc (Biretta et al. 1991) and $B_m = 4.59$ mG (Owen et al. 1989), we see in Figure 2 (*top*) that the ν_b-value calls for a fluctuation level of $b \simeq 1 \times 10^{-3}$, consistent with the assumption of the small-amplitude disturbance (§ 2.1); that is why this b-level has been taken into account for Figure 1 (*bottom*).

Let us now evaluate the F_ν spectral index, which is well defined in the transitive frequency range between ν_b and ν_c^*. Recalling the canonical index $\alpha_1[= (p-1)/2]$ for $\nu < \nu_b$, for heuristic purposes, we give the definition of $\alpha_2 \equiv -\Delta \log F_\nu / \Delta \log \nu$, where $\Delta \log F_\nu = -\alpha_1 \Delta \log \nu + \log \phi$ and $\Delta \log \nu [= \log(\nu_c^*/\nu_b)] = [2\mu - (\beta-1)/2] \log(\tilde{l}D/\lambda_c)$. That is, the index is found to be expressed in the form

$$\alpha_2 = \frac{p-1}{2} + \frac{p+1}{2} \left[\frac{4\mu(\beta, \beta')}{\beta - 1} - 1 \right]^{-1} \tag{3}$$

---

[1] Eq. (2) reflects the ratio of the averaged magnetic intensity of small to large filaments; that is, $\left\{ \left[\int_{\lambda_{\rm min}}^{\lambda_c} \lambda^\beta (d\lambda/\lambda^2) \right]^{1/2} \left[\int_{\lambda_c}^{\tilde{l}D} \lambda^\beta (d\lambda/\lambda^2) \right]^{-1/2} \right\}^{(p+1)/2} \simeq \phi$ in a good approximation for $\lambda_{\rm min} \ll \lambda_c \ll \tilde{l}D$, where $\lambda_{\rm min}$ is the minimum scale of λ, which might be compared to the skin depth (§ 3.3).

for $\mu > (\beta - 1)/4$. Note that equation (3) is generic, as it is independent of $\lambda_c/\tilde{l}D$ and thereby independent of any magnetic field parameters (such as B_m and b). The second term of the right-hand side that just represents the steepening of the spectrum is coupled, through p, with the first term, to deviate from 1/2 ($\alpha_2 = \alpha_1 + 1/2$) for a conventional synchrotron model (Kardashev 1962; Longair 1994). As seems more reasonable, the α_2 value can be compared to the spectral index measured in a X-ray band.

In Figure 3, for $\beta' = 5/3$, we plot, for convenience, $\alpha_2(\mu = \mu_{\rm syn})$ as a function of β, for a given α_1 in the range of $0.5 - 0.8$. Clearly, one can find that for $\alpha_1 = $ const, the value of α_2 monotonically increases as the value of β increases. As denoted in Appendix A, by inverting equation (3) we can express β as a function of α_1, α_2, and β'. When assigning the observational indices of $\alpha = 0.67$ (in the radio-optical band) and 1.46 (in the *Chandra* regime of $0.5 - 7.5$ keV) to α_1 and α_2, respectively, equation (A1) with equation (A2) gives $\beta = 4.3$ for a reliable case of $\beta' = 5/3$ (see also Fig. 3). This β-value, somewhat larger than the value of ~ 2 expected in an early stage of the current filamentation instability (Montgomery & Liu 1979), is amenable to the updated result of a three-dimensional kinetic simulation that revealed the marked steepening of spectrum in a fully developed nonlinear phase (Silva et al. 2003; see their Fig. 3), reflecting accumulation of self-organized larger filaments via the violent coalescence of smaller filaments (Honda et al. 2000a,b). In fact, the observational results indicate that the X-ray spectrum tends to be steepened when departing from the active galactic core (Marshall et al. 2002), while the radio-optical index likely remains constant (Perlman et al. 2001); for the spectral data sets of, e.g., knot *HST*-1 [$(\alpha_1, \alpha_2) = (0.71, 1.29)$], knot D $(0.69, 1.33)$, and knot A $(0.67, 1.57)$, equation (A1) yields $\beta = 2.4$, 2.8, and 6.6, respectively. The gradual increase of β (departing from ~ 2 at the innermost knot) might, more or less, reflect the actual dynamic evolution of a filament cluster involving the coalescence, which has originally been inspected by Owen et al. (1989).

The minor component of electrons bound to the small filaments with weak $|\mathbf{B}|$ makes a negligible contribution to F_ν in the region of $\nu < \nu_c^*$, but instead, the electrons can escape from the small filaments, to be additionally accelerated above γ_c^* (§§ 2.1 and 3.1). The energetic synchrotron emission from the free (not persistently bound) electrons tends to be diffusive, and the spectral index, α_3, could be close to β (independent of p; Toptygin & Fleishman 1987; Fleishman 2006). In the case in which around the critical frequency of ν_c^* the flux density level of the diffuse component is not negligibly smaller than that for the coherent one, e.g. for $\alpha_3 > \alpha_2$ the synchrotron spectrum is further steepened above ν_c^* to extend the gamma-ray tail. More on this topic is discussed in § 3.3 and in Appendices A and B.

3. ENERGY REBOOST TO THE PeV RANGE AND GAMMA-RAY EMISSION

Below we consider the additional DSA of the injected electrons undergoing the *nongyrational* motion in the filamentary plasma. We evaluate the achievable highest energy (§ 3.1) and the upper limit of the photon frequency (§ 3.2), and argue a condition for which the high-frequency tail of the gamma-ray synchrotron spectrum could be extended (§ 3.3).

3.1. *Cutoff Lorentz Factor of Energetic-Tail Electrons*

The sufficient condition for which the free electrons can be additionally accelerated in situ is that the acceleration time must be shorter than that for the conventional DSA of gyrating electrons (for the necessary condition, see §§ 2.1 and 5). In the high-energy regime compared to high-β plasma state, the free electrons spaciously meander, suffering successive small deflections by the quasi-static magnetic fields fluctuating in the zeroth order (sustained by bulk current filaments). The fields of many fine filaments can be characterized by the rms strength of $B = (\langle |\mathbf{B}|^2 \rangle)^{1/2}$, where $\langle \cdots \rangle$ indicates an average on the transverse two-dimensional plane of the filaments; an average vector of the local fields likely vanishes in the interior of the jet such that $|\langle \mathbf{B} \rangle| \ll B$, whereby the gyroradius can be no longer well defined. The key kinetic property in this energetic regime is that the free electrons quickly lose coherence of the trajectory in the stochastic medium. For the off-resonant scattering diffusion (Honda & Honda 2005a), the correct ordering of the mean free path is $\ell_e \sim \epsilon^2/(e^2 B^2 \tilde{l} D)$; here note that its anisotropy is small, according to the three-dimensional rms deflection. The ratio of the mfp to $r_{g,e}$ can be expressed as

$$\frac{\ell_e}{r_{g,e}} \sim 10^{-3} \frac{\gamma}{10^9} \frac{10\ \mu\mathrm{G}}{B} \frac{100\ \mathrm{pc}}{\tilde{l} D}. \tag{4}$$

It is evident that there is a wide parameter range in which $\ell_e < r_{g,e}$.[2] For example, for the ordering of $B \sim |\mathbf{B}|_{\lambda \sim \lambda_c} \sim 10\ \mu$G and $\tilde{l} D = 110$ pc (Biretta et al. 1991), the relation of $\ell_e < r_{g,e}$ is safely satisfied in the range of $\gamma \leq 10^{11}$. The shorter mfp (in the shock normal direction) is essential for more rapid back-and-forth across the shock, resulting in a shorter DSA timescale.

[2]Relating to a major difference from the ion kinetics that was examined in the preceding work (Honda & Honda 2004a), one can find the inequality relation of $\ell_e/r_{g,e} \ll \ell_i/r_{g,i} \leq \ell_p/r_{g,p}$, where the subscripts "$i$" and "$p$" indicate arbitrary ions and protons, respectively. In this sense, the quick loss of the coherence in electron motion is more pronounced than that in ion motion.

If we allow $\tilde{l}$ to take a value less than unity, the modified version of the mean acceleration time for the electrons is found to give the scaling of

$$t_{\rm acc} \simeq 10 \left(\frac{\gamma}{10^{11}}\right)^2 \left(\frac{10\ \mu{\rm G}}{B}\right)^2 \frac{100\ {\rm pc}}{\tilde{l}D} \left(\frac{0.5c}{U}\right)^2\ {\rm yr}. \tag{5}$$

The numerical factor of equation (5) is correct for $\beta = 4.3$ and $r = 3.2$ (expected at knot A), although it is merely weakly dependent on these parameters. For, e.g., $B \sim 10\ \mu$G, $\tilde{l}D = 110$ pc, and $U = 0.5c$, the acceleration timescale (eq. [5]) is, at $\gamma = \gamma_c^* (\sim 10^9 - 10^{10})$, favorably shorter than the critical DSA timescale of $[r/(r-1)](cr_{g,e}/U^2) \sim 1 - 10$ yr for the Bohm diffusion limit.[3] Importantly, this ensures that the sufficient condition for further energization of the escape electrons with $\gamma = \gamma_c^*$ (and less) is satisfied. In particular, the critical energy $\gamma_c^* mc^2$ may be associated with the injection energy for the additional DSA (§ 2.1), and the conventional DSA of the gyrating electrons in the escape tracks (illustrated in Fig. 1, *bottom*) can be regarded as the "preaccelerator" in the envisagement of the two-step DSA. Since the shorter $t_{\rm acc}$ of equation (5) can be retained up to the very energetic regime of $\gamma \sim 10^{11}$ (in conformity with $\ell_e < r_{g,e}$), we expect that two electron populations mediated by the injection threshold, namely, the major low-energy and minor high-energy components, will be established. Recall here that for the Fermi (type I) fashion, the resulting index p (for the power-law $dn/d\epsilon$ distribution) is independent of the diffusion coefficient, depending solely on the scattering center compression ratio r (§ 2.1). Accordingly, for the present model supposing ubiquitous Fermi operation in the two energy levels, it is, at least for a high Mach number case, expected that the power-law distribution likely has a common p (Vainio 1999; Schlickeiser 2002).

As usual, the additional DSA of the injected electrons operates as long as they are confined in the accelerator, where the electron kinetic energy can increase until $t_{\rm acc}$ asymptotically approaches the radiative loss times. This spatiotemporal limit truncates the power-law tail of such a $dn/d\epsilon$ distribution. We note that the spatial limit may be denoted as $\ell_e \sim D$, instead of $r_{g,e} \sim \lambda$ for the pre-DSA, and as for the synchrotron loss, the diffuse effects could be nonnegligible (Toptygin & Fleishman 1987; Fleishman 2006). We here take, for convenience, the harmonic average of the synchrotron and IC cooling times to get

[3] Concerning the limitation of $t_{\rm acc}$ that depends on the diffusion coefficient, there is a general constraint for which the diffusion speed of electrons must be larger than U (Jokipii 1987; Honda & Honda 2005b). For nonrelativistic shocks, indeed, this constraint turns out to be satisfied, as far as the electron mfp in the shock's normal direction does not greatly exceed the characteristic length of the density gradient. Also, equation (5) cannot take unlimitedly smaller values with decreasing γ, because the gyrotrapping effects of cold electrons in the local magnetic fields make the approximation of $|\langle \mathbf{B} \rangle| \ll B$ worse. The lower limit of γ reflects the energy required for escape from the local magnetic traps.

$t_{\rm acc} = t_{\rm syn}[1 + a\tilde{\tau}(\sigma_{\rm KN}/\sigma_{\rm T})]^{-1}$, where $t_{\rm syn}$ is the diffuse synchrotron time derived in Appendix B, $\tilde{\tau}$ is a dimensionless factor (see eq. [B4]), $a \equiv 8\pi u_{\rm ph}/B^2$, and $\sigma_{\rm KN}/\sigma_{\rm T}$ is the ratio of the Klein-Nishina and Thomson cross sections (e.g., Longair 1992, 1994). Note that this time-balance equation does not explicitly contain B, because both $t_{\rm acc}$ and $t_{\rm syn}$ have a common dependence of being proportional to B^{-2}. Solving the spatiotemporal balance equation for γ, given $\tilde{l}D$, U, a, and the characteristic frequency of target photons in the comoving frame, ν_t (involved in $\sigma_{\rm KN}$), yields the achievable maximum (cutoff) Lorentz factor of an accelerated electron, defined as $\gamma_c \equiv \min\left(\gamma|_{t_{\rm acc}=t_{\rm loss}}, \gamma|_{\ell_e=D}\right)$.

In Figure 4, for the standard parameter set of $\tilde{l}D = 110$ pc and $U = 0.5c$ (§ 2), the numerical solutions, γ_c, are plotted as a function of ν_t in the parameter range of $10^1 \leq a \leq 10^6$. In any case, we find that the spatial limit plays a nondominant role in determining γ_c (thereby, $\gamma_c = \gamma|_{t_{\rm acc}=t_{\rm loss}}$), in contrast to the previous case of determining γ^* (§ 2.1). For the larger $a\tilde{\tau}$ value, we see that in the Thomson limit of $h\nu_t \ll mc^2/\gamma_c$, where h is the Planck constant, the values of γ_c take constants because $\sigma_{\rm KN}/\sigma_{\rm T} \simeq 1$, while for $h\nu_t \gtrsim mc^2/\gamma_c$, in which $\sigma_{\rm KN}/\sigma_{\rm T} < 1$, the Klein-Nishina effect enhances the value of γ_c. However, γ_c does not unlimitedly increase, but eventually saturates, because of the dominance of the diffuse synchrotron cooling loss, to take a constant value. For variations of ν_t, the allowed domain of the other variables can be thus written as follows:

$$1 \geq \frac{\gamma_c}{5\times10^{10}}\left(\frac{100\ {\rm pc}}{\tilde{l}D}\right)^{1/3}\left(\frac{0.5c}{U}\right)^{2/3} \geq \frac{1}{(1+a\tilde{\tau})^{1/3}}. \tag{6}$$

Note that the upper bound and $a\tilde{\tau} \ll 1$ reflect the diffuse synchrotron limit and the lower bound for $a\tilde{\tau} > 1$ reflects the Thomson limit.

In the region in which $B < 1$ mG, the EC scatterers, including the starlight and dust emission (§ 2.1), can lead to $a > 1$ for $1 \lesssim \Gamma < 10$. As seen in Figure 4, however, in their characteristic frequencies of $\nu_t \sim 10^{14}\Gamma$ Hz (stars) and $3\times10^{13}\Gamma$ Hz (dust) the values of γ_c turn out to be limited by the diffuse synchrotron cooling rather than the IC cooling, for the displayed range of $a \leq 10^6$ that would cover the conceivable a-values. This is because the Klein-Nishina effects prolong the IC timescale beyond the diffuse synchrotron time. Although the CMB provides a lower target frequency ($\nu_t \simeq 2\times10^{11}\Gamma$ Hz) that tends to fade the Klein-Nishina effects, again it will play a negligible role in determining γ_c, because $a < 1$; the SSC process is also ignorable, as the source arranges a lower $u_{\rm ph}$ and higher ν_t compared to those of the above EC sources (Stawarz et al. 2003). Consequently, for the standard value of $\beta = 4.3$ and another possible value of $\beta = 6.6$ (at knot A; § 2.2), we obtain $\gamma_c \simeq 5\times10^{10}$ (Fig. 4) and 4×10^{10}, respectively, exceeding γ_c^*, and then the diffuse synchrotron timescales are, for example, for $B \sim 10$ μG, estimated as $t_{\rm syn}$ ($\sim t_{\rm acc}$) ~ 2 yr (eq. [5]) and 1 yr, respectively. Even if the $\tilde{l}$-value deviates from unity ($\tilde{l} \lesssim 1$), the decrease of these γ_c-values is not so significant on account of the dependence of $\gamma_c \propto \tilde{l}^{1/3}$.

3.2. *Inverse Compton Gamma-Ray Cutoff*

The electrons concomitant with the truncated power-law distribution scatter the target photons with frequency ν_t boosting them to higher frequency regions. Of particular interest is the achievable highest frequency of the scattered photons, since a significantly large value of γ_c is accomplished in the present scenario. This is the subject of truncation of the gamma-ray spectrum.

In Figure 5 we plot the highest (cutoff) frequency of the IC radiation (in the comoving frame), $\nu_{\rm ic,c}$, as a function of ν_t in the parameter range of $10^1 \leq a \leq 10^6$. The values of $\tilde{l}D$ and U are chosen to be the same as those in Figure 4. In the high-energy and high-frequency region of $h\nu_t \gg mc^2/(4\gamma_c)$, we find that $\nu_{\rm ic,c} \simeq \gamma_c mc^2/h$, while for $h\nu_t \ll mc^2/(4\gamma_c)$, which covers the Thomson limit, $\nu_{\rm ic,c} \simeq 4\gamma_c^2\nu_t$. Note that in a Klein-Nishina regime satisfying $t_{\rm ic} > t_{\rm syn}$, where γ_c takes a value independent of ν_t (Fig. 4), the former expression of $\nu_{\rm ic,c}$ ($\propto \gamma_c$) is independent of ν_t, as is obviously seen in Figure 5. The scaling of this upper limit is written in the simple form

$$\nu_{\rm ic,c} \simeq 6 \times 10^{30} \left(\frac{\tilde{l}D}{100\ {\rm pc}}\right)^{1/3} \left(\frac{U}{0.5c}\right)^{2/3}\ {\rm Hz}. \tag{7}$$

Apparently, this is just the case involved in the EC scenarios due to the stellar and dust emissions with $\nu_t \sim 10^{14}\Gamma$ Hz and $3 \times 10^{13}\Gamma$ Hz, respectively (§ 3.1, Fig. 5), to safely give the ordering of $\nu_{\rm ic,c} \sim 10^{30}$ Hz for the reasonable parameter range. Again we point out the weak $\tilde{l}$ dependence and the B independence of equation (7), and that the CMB-based EC and SSC mechanisms will not greatly change the $\nu_{\rm ic,c}$-value. As a consequence, we can claim that the $\nu_{\rm ic,c}$-value multiplied by an appropriate Doppler factor, which is of order unity in the present regime, provides a common cutoff of the IC radiation from the source. Concerning the observability of the very energetic photons, the absorption in extragalactic background light with subsequent pair production (Nikishov 1962; Gould & Schréder 1966) will be significant in spite of the proximity. The relevant issues, including applicability to more distant radio galaxies, are discussed in § 5.

In Figure 6, for $\tilde{l}D = 110$ pc and $U = 0.5c$, we present the model νF_ν spectra of the possible IC radiation due to the EC target with $\nu_t = 10^{14}$ Hz (stars) and, for convenience, the synchrotron radiation for the corresponding case of $\beta = 4.3$ (*solid curve*), and another case with $\beta = 6.6$ (*dotted curve*) as a comparison. The synchrotron spectra have been best fitted to the observational data of near-infrared to optical (at the knot A shock; Perlman et al. 2001) and X-ray bands (knot A; Marshall et al. 2002). As for the IC radiation component, we plot the intrinsic (source) spectrum for the possible cases of $a = 10^{-2}$ (*dot-dashed curve*) and 10^{-1} (*dashed curve*), as accommodated by the data recently observed by the HESS telescope

(Beilicke et al. 2005) that are considered to reflect a quiescent epoch of the (unresolved) gamma-ray source. Note that the chosen a-values will sufficiently reflect the uncertain value of $u_{\rm ph} \gtrsim 10^{-9}$ ergs cm^{-3} and rms strength of the fields that trap the major electrons emitting the synchrotron photons with the frequency $\sim \nu_b$ (at which νF_ν takes the peak). As seen in Figure 6, below the break frequency of IC gamma rays, the ν dependence of νF_ν coincides with that for the synchrotron continuum [i.e., $\nu F_\nu \propto \nu^{(3-p)/2} = \nu^{0.33}$], and the spectrum takes the local maximum value of $\nu F_\nu \simeq 4 \times 10^{10}$ Jy Hz for $a = 10^{-1}$ at the break frequency of $\sim 10^{25}$ Hz. Above the break, νF_ν is significantly suppressed due to the Klein-Nishina effects, followed by the asymptotic dependence of $\nu F_\nu \propto \nu^{-(p-1)} \ln \nu$ ($\sim \nu^{-1.2}$ for a spectral fit), and ends up with the cutoff at $\nu_{{\rm ic},c} \simeq 6 \times 10^{30}$ Hz (eq. [7]). We note that changing the β-value to 6.6 leads to a slight shift of the cutoff to $\nu_{{\rm ic},c} \simeq 5 \times 10^{30}$ Hz (not shown in the figure). In sub-GeV to GeV regimes, the curve for $a = 10^{-1}$ reaches the sensitivity limit of the LAT instrument (Large Area Telescope) on board the *Gamma-Ray Large Area Space Telescope* (*GLAST*).

In regard to the synchrotron spectra, the cases of $\beta = 4.3$ and 6.6 reproduce, via equation (3), for $(\alpha_1, \beta') = (0.67, 5/3)$, $\nu F_\nu \propto \nu^{-0.46}$ and $\nu^{-0.57}$ in the transitive frequency range that covers the *Chandra* band (Marshall et al. 2002), giving $\nu_b \simeq 7 \times 10^{14}$ and 1×10^{15} Hz, respectively; and in turn, for the self-consistently determined b-levels (about 1×10^{-3} and 2×10^{-3}, respectively, for the typical $\tilde{l}D$ and B_m; § 2.2), we numerically find $\nu_c^* \simeq 1 \times 10^{21}$ Hz (Fig. 2, *middle*) and 2×10^{21} Hz, as well as $\phi \simeq 1 \times 10^{-5}$ (Fig. 2, *bottom*) and 3×10^{-6}, respectively. As seen in Figure 6, for example, for the case of $a = 10^{-1}$, the νF_ν levels of the synchrotron component are, above the frequencies of 7×10^{19} and 3×10^{19} Hz (for each of the β-value cases), overcome by those of the IC component, and at $\nu = \nu_c^*$, they are lower than the IC level by a factor of about 4×10^{-2} and 1×10^{-2}, respectively.

3.3. *On the Gamma-Ray Tail of the Synchrotron Spectrum*

Regarding the energetic synchrotron radiation above ν_c^*, we are concerned with the following two possible channels of the related electron kinetics in actual circumstances: (1) the additionally accelerated electrons mainly retain the meandering motion without getting trapped in the filaments, and (2) the electrons (with energy ϵ) are transported to be trapped in the larger filaments with the size (λ) in the range of $\lambda_c < 2r_{g,e}(\epsilon) < \lambda$ ($\leq D$) and are cooled down through the gyration with $r_{g,e}$. For case 1, the diffuse synchrotron spectrum exhibiting $F_{\nu,d} \propto \nu^{-\beta}$ can appear in a region of $\nu > \nu_c^*$. At $\nu = \nu_c^*$, the flux density ratio of

the diffuse to the coherent synchrotron component is found to scale as

$$\left(\frac{F_{\nu,d}}{F_\nu}\right)_{\nu=\nu_c^*} \simeq 2\times10^{-15}\left(\frac{10^{-3}\ \mathrm{pc}}{\langle\lambda\rangle}\right)^{3.3}\left(\frac{\gamma_c/\gamma_c^*}{10}\right)^{7.3}\left(\frac{10\ \mu\mathrm{G}}{B}\right)^{3.3} \tag{8}$$

for $\beta = 4.3$ (see eq. [B5] for an arbitrary β). For the case reflected in Figure 1 (*bottom*) and for the diffuse synchrotron limit (Fig. 4), we have $\gamma_c/\gamma_c^* \simeq 7$ and B ($\sim |\mathbf{B}|_{\lambda=\lambda_c}$) $\sim$ 5 μG, whereupon in equation (8), the continuity condition of $(F_{\nu,d}/F_\nu)_{\nu=\nu_c^*} = 1$ requires a considerably small size $\langle\lambda\rangle \sim 3\times10^{-8}$ pc (9×10^{10} cm). Although the $\langle\lambda\rangle$-value is much larger than the order of magnitude of the skin depth ($\sim 10^6$ cm for a plasma density of $\sim 10^{-1}$ cm^{-3}; Owen et al. 1990; Di Matteo et al. 2003), it is still unclear whether a large number of the filaments that are much smaller than $\tilde{l}D$ can actually exist or not. For $(F_{\nu,d}/F_\nu)_{\nu=\nu_c^*} \ll 1$, the critical frequency ν_c^* can be regarded as a cutoff accompanied by the exponential-like decay of F_ν, and such a case is shown in Figure 6, as an example.

For case 2, in which the orbit stochasity of the rms deflection becomes incomplete, the diffuse synchrotron spectrum will be modified such that the emission of the fundamental mode appears to be preferentially pronounced. For an estimation of the effective frequency ν_c, one can employ the simple formula ($\propto \gamma_c^2|\mathbf{B}|$), intending to make a comparison with the previously suggested cutoff for coherent synchrotron radiation (§ 1). Combining equation (6) with the formula yields

$$1 \geq \frac{\nu_c}{1\times10^{24}\ \mathrm{Hz}}\frac{100\ \mu\mathrm{G}}{|\mathbf{B}|_{\lambda>\lambda_c}}\left(\frac{100\ \mathrm{pc}}{\tilde{l}D}\right)^{2/3}\left(\frac{0.5c}{U}\right)^{4/3} \geq \frac{1}{(1+a\tilde{\tau})^{2/3}}. \tag{9}$$

In equation (9), the upper limit (or $a\tilde{\tau} \ll 1$), achievable in the knot A environment (§ 3.1), gives a scaling of $\nu_c \propto |\mathbf{B}|_{\lambda>\lambda_c}(\tilde{l}D)^{2/3}U^{4/3}$, and then, for given values of $\tilde{l}D = 110$ pc and $U = 0.5c$, the expected range is $\nu_c \geq 10^{23}$ Hz for $|\mathbf{B}|_{\lambda>\lambda_c} \geq 10\ \mu$G. Because of the large value of γ_c, the value of ν_c is found to be strikingly larger than the previous values of $\sim 10^{15}$ Hz (Keel 1988; Pérez-Fournon et al. 1988; Meisenheimer et al. 1996; Stiavelli et al. 1997), which could be deduced from a simple DSA model assuming the resonant scattering diffusion of the electrons confined in a uniform jet (e.g., Biermann & Strittmatter 1987 for a parallel shock case).

4. *Variability of the Broadband Spectrum*

To complement the model predictions, we give a discussion of the variability of the broadband spectrum, shown in Figure 6. In the low-frequency bands associated with synchrotron radiation, it is expected that the light curves reflect the spatial inhomogeneity of

the interior. The synchrotron emissions from the escaped electrons with Lorentz factors above $\gamma_e^* = [eB_m\tilde{l}D/(2mc^2)](\lambda/\tilde{l}D)^{(1+\beta)/2}$ (i.e., above the dotted line in Fig. 1, *bottom*) will exhibit the high-frequency variation with a typical light-crossing time of order $\sim \lambda/c$. In this regime, the highest (cutoff) frequency of the power spectrum might be compared to the plasma frequency. On the other hand, the electrons in the quasi-secular trap tracks (the shaded regions in Fig. 1, *bottom*) cannot freely cross the filaments, in which, instead of such a variation with a timescale of λ/c, the low-frequency variation due to the shock intermittency that might reflect the activity of the galactic central engine (Biretta et al. 1995) could appear, conforming to the $1/f - 1/f^2$ flicker-noise spectrum (e.g., Kataoka et al. 2001). The bound electrons that emit a synchrotron photon with frequency ν have a Lorentz factor of $\gamma = [4\pi mc\nu/(3eB_m)]^{1/2}(\lambda/\tilde{l}D)^{(1-\beta)/4}$. Equating $\gamma(\lambda,\nu)$ to $\gamma_e^*(\lambda)$, we find the solution λ (as a function of ν), which is for convenience labeled as λ_b (the high-frequency variation relies on the spatioscale of $\lambda < \lambda_b$). The quantity $c/\lambda_b \equiv f_b$ then characterizes the frequency that discriminates between the aforementioned high- and low-frequency regions of the power spectrum for the ν-band light curve. This key frequency, analogous to the bend-over frequency of the broken power spectrum for blazar light curves (Appendix C), is found to scale as

$$f_b \simeq 2\times10^{-8}\left(\frac{10^{15}\ \mathrm{Hz}}{\nu}\right)^{0.14}\left(\frac{B_\mathrm{m}}{1\ \mathrm{mG}}\right)^{0.43}\left(\frac{100\ \mathrm{pc}}{\tilde{l}D}\right)^{0.71}\ \mathrm{Hz} \tag{10}$$

for $\beta = 4.3$ (see eq. [C1] for the generic expression). Note the very weak ν dependence of f_b, in accordance with the feature of the blazar light curves. For the parameter set of $B_m = 4.59$ mG and $\tilde{l}D = 110$ pc, equation (10) gives $f_b \simeq 4\times10^{-8}$ Hz and 2×10^{-8} Hz for $\nu = 10^{15}$ Hz (optical/UV) and 10^{18} Hz (X-ray), respectively. We note that for $\beta = 6.6$, these f_b-values shift down to 5×10^{-9} Hz and 3×10^{-9} Hz, respectively. As a consequence, the model predicts the characteristic variation with a 1 yr and 10 yr timescale (for $\beta = 4.3$ and 6.6, respectively), longer than a day timescale for typical blazar jets (Appendix C; eq. [C1]).

Concerning the MeV/GeV and sub-TeV/TeV gamma-ray light curves, the high-frequency variation (reflecting the filament size) cannot appear, as the bound electrons in the quasi-secular trap tracks dominantly contribute to Comptonize the target photons. The variation could solely reflect the intermittence of the shock accelerator in the flicker-noise regime. In the EC model supposing a stationary u_ph value, it then appears that the gamma-ray variation must correlate with the variation of the synchrotron spectrum in the low-frequency (flicker noise) regime below f_b. This feature will provide a constraint to explain the data of the High Energy Gamma Ray Astronomy (*HEGRA*) experiments (Aharonian et al. 2003) that seem to reflect the flaring phase of the source (see Fig. 6). Even though the other scenarios (Bai & Lee 2001 for the SSC; Protheroe et al. 2003 and Reimer et al. 2004 for the synchrotron-proton blazar [SPB] model; Stawarz et al. 2006a for the EC involving nuclear

activity) could also be candidates for explaining the higher flux level and variation, we can claim that the present simple model will guarantee the level shown in Figure 6, which is compatible with the lower levels recently confirmed by HESS (Beilicke et al. 2005), as well as consistent with the updated Whipple 10 m telescope upper limit (Le Bohec et al. 2004).

5. DISCUSSION AND CONCLUSIONS

In the present conception, the lack of the filaments with $\lambda < \lambda_c$ leads to the failure of the transition injection followed by the additional DSA. Moreover, even if fine filaments exist, the large value of $\langle\lambda\rangle$ lowers the $F_{\nu,d}$ level, as is deduced from equation (8) (or eq. [B5]). It is, therefore, important to confirm the presence of such a small scale in the actual jet. In this aspect, finding f_b and the high-frequency extension of the power spectrum (for the observed light curve; § 4) provide the implication of the presence of the small scale of $\lambda < \lambda_b$, and in addition, the truncation of the power spectrum just reflects the actual smallest value of λ, whose lower limit is expected to be on the order of $\sim 10^6$ cm (§ 3.3). Another feasible method is availing of the property according to which emission from the electrons in the stochastic medium could be unpolarized. The threshold frequency above which the polarization decreases is estimated as $\nu_{\rm th} = (3/4\pi)(|e\mathbf{A}|/mc^2)^2(|e\mathbf{B}|/mc)$, where $\mathbf{B} = \nabla\times\mathbf{A}$, to give the corresponding coherence length that scales as $\lambda \simeq 2\times10^{-3}\,(\nu_{\rm th}/10^{15}\ {\rm Hz})^{1/2}\,(10\ \mu{\rm G}/|\mathbf{B}|)^{3/2}$ pc. Combined with the expression of $|\mathbf{B}|$ (as a function of λ), the scaling is recast to

$$\lambda \simeq 0.6\left(\frac{\nu_{\rm th}}{10^{15}\ {\rm Hz}}\right)^{0.14}\left(\frac{1\ {\rm mG}}{B_m}\right)^{0.43}\left(\frac{\tilde{l}D}{100\ {\rm pc}}\right)^{0.71}\ {\rm pc} \tag{11}$$

for $\beta = 4.3$. In particular, for the knot A parameters of $\tilde{l}D = 110$ pc and $B_m = 4.59$ mG, equation (11) reduces to $\lambda \simeq 0.3(\nu_{\rm th}/10^{15}\ {\rm Hz})^{0.14}$ pc, simply having a weak dependence on $\nu_{\rm th}$; then, for example, for the optical range of $\nu_{\rm th}$ (Perlman et al. 1999), we have $\lambda \sim (2-3)\times10^{-1}$ pc, smaller than $\lambda_c \simeq 2$ pc (or 7 pc for $\beta = 6.6$). The direct measurement of λ seems to be difficult even by the modern *Hubble Space Telescope* with a spatioresolution of $0.1''$; viz., 7.8 pc at the distance to M87 (~ 16 Mpc; Tonry 1991), while the λ_c-value may be comparable to the spatioresolution.

In conclusion, we have given a full argument in favor of regarding the M87 jet/knot A as a hard X-ray and gamma-ray emitter, owing to the Pevatron electron accelerator comprising the two-step DSA based on the filamentary jet model. In a plausible case in which the Alfvénic fluctuations superimposed on the local mean magnetic fields (sustained by the bulk current filaments) are in a Kolmogorov turbulent state, the observed X-ray spectral index of 1.46 (or 1.57) (Marshall et al. 2002) has been reproduced for the spectral index of filamen-

tary turbulence of $\beta = 4.3$ (6.6), which is amenable to the results of the kinetic simulations that solve a long time evolution of filamentation instability. For the typical parameter set of a shock speed of $0.5c$ (Biretta et al. 1995), a field inclination angle of 60° (e.g., Owen et al. 1989; Capetti et al. 1997; Heinz & Begelman 1997). a compression ratio of 3.2 (compatible with the radio-optical index of 0.67; Perlman et al. 2001), a filament correlation scale compared to the jet diameter of 110 pc (Biretta et al. 1991), and the magnetic intensity of an outer scale filament of 4.59 mG (Owen et al. 1989), we have self-consistently determined the Alfvénic fluctuation level and found that the synchrotron cutoff most likely appears at 1×10^{21} Hz (for $\beta = 4.3$; 2×10^{21} Hz for $\beta = 6.6$), where the flux density is, by a factor of 1×10^{-5} (6×10^{-6}), lower than that inferred from the extrapolation of the radio-optical continuum. For the optical/UV and X-ray light curves, the bend-over frequencies of their power spectra have been estimated as 4×10^{-8} Hz (5×10^{-9} Hz) and 2×10^{-8} Hz (3×10^{-9} Hz), respectively. The additional DSA incorporated with the transition injection turns out to require fine filaments with a transverse size smaller than 2 pc (7 pc) to boost the Lorentz factor of a free electron to 5×10^{10} (4×10^{10}), independent of the rms magnetic field strength of the filaments. The intrinsic cutoff frequency of the conceivable IC (EC and SSC) radiation is worked out at 6×10^{30} Hz (5×10^{30} Hz), which just reflects the uppermost electron energy of ~ 20 PeV. It is expected that the MeV/GeV and sub-TeV/TeV gamma-ray light curves solely reflect the intermittence of the shock accelerator in the flicker-noise regime.

The present conception for the generation of very energetic emission from the large-scale jet will constitute a frontier, complementary to the other scenarios that predict emission from the unresolved galactic core (Protheroe et al. 2003 and Reimer et al. 2004 for the SPB model as a misaligned BL Lac object). Concerning potential applicability to more distant sources, if the similarity of blazar variability to the present one (eq. [10]; Appendix C) is confirmed in future observations, the filamentary jet model could be useful for inferring the detailed structure of blazar jets. It then follows that the generic modeling can be used to reinforce an interpretation of the intrinsic νF_ν spectra that have been less well theoretically studied so far. Even for the nearby galaxy M87 ($z = 0.00427$), the cosmic infrared background (CIB) will opaque the gamma rays with energies in the range $10 - 100$ TeV, although the uncertainty of the extragalactic CIB level makes it difficult to accurately determine the optical depth (Coppi & Aharonian 1997; Protheroe & Meyer 2000; Aharonian 2001) and thereby the observed cutoff (the expected range is indicated in Fig. 6). By contrast, the PeV photons ought to suffer the absorption dominantly by the CMB, so that their mfp can be predicted with very high accuracy, provided that the Lorentz invariance remains even in the ultrahigh energy region. In any case, the present model spectrum is readily referable to the radio-loud sources within ~ 100 Mpc, for which the extragalactic background (CMB, CIB) light is almost transparent for the sub-TeV (TeV) photons dominantly carrying the

IC gamma-ray flux, whereas for the more distant sources the observed gamma-ray cutoffs could shift to a lower frequency region, down to the lower limit that seems to appear around ~ 10 GeV (Kneiske et al. 2004).

Relating to this perspective, the pair-cascade radiation triggered by the photon-photon annihilation potentially contributes to raising the extragalactic gamma-ray background level (Sreekumar et al. 1998; Strong et al. 2004). When assuming a stellar emission level, the gamma-ray luminosity apparently depends on the rms magnetic field strength; that is, the complexity of the filamentary turbulent state (including a spectral index deviating from that of classical hydromagnetic turbulence; eq. [A1]). But the contribution from all Fanaroff-Riley (FR) type I radio galaxies containing X-ray jets is expected not to exceed the one from blazars (Kneiske & Mannheim 2005) as long as the rms strength is, on average, not much smaller than the equipartition value (like the case shown in Fig. 6 for $a \leq 10^{-1}$), along with the arguments invoking the luminosity function (see Stawarz et al. 2006b for the details). Particularly, for the smaller power index of the filamentary turbulence, the rms strength of the fields that trap major electrons constituting the synchrotron νF_ν peak tends to be comparable to the uppermost value of ~ 1 mG for the outer scale filament, wherein the smaller contribution of at most 1 % is merely guaranteed. These arguments are not affected by the shift of the intrinsic cutoff in the PeV range, as the dominant contribution commonly owes to the (sub-)TeV photons constituting the local maximum of νF_ν. To verify the predictions, in addition to the survey of hidden sources by future high-sensitivity detectors, comprehensive measurements of the filamentary turbulence and its spectrum as well would be of powerful use (e.g., Carilli & Barthel 1996), bringing on some interesting information, arguably linked to synchrotron spectra (§ 2.2; Fig. 3). Modern laboratory experiments of high-intensity laser-matter interaction, which can reproduce the similar turbulent state (e.g., Wei et al. 2004), might be also available for resolving the complexities in detail.

A. THE EXPRESSION OF THE SPECTRAL INDEX OF FILAMENTARY TURBULENCE

For instruction, here we write down the expression of the power-law spectral index of magnetized filamentary turbulence, β, as a function of the indices α_1, α_2 ($> \alpha_1$), and β' ($\neq 1$). Again, note that α_1 (for $\nu < \nu_b$) and α_2 (for $\nu_b < \nu < \nu_c^*$) could be typically compared to the radio-optical and X-ray indices, respectively, and β' indicates the power-law index of the Alfvénic fluctuation disturbing the zeroth-order magnetic field (permeating through the current filaments). If we make use of equation (1) for the ordinary case of $\mu = \mu_{\rm syn}(\beta, \beta')$,

the inversion of equation (3) readily gives

$$\beta(\alpha_1, \alpha_2, \beta') = \frac{x(\alpha_1, \alpha_2) + x_a(\beta')}{x(\alpha_1, \alpha_2) - 3x_a(\beta')}, \tag{A1}$$

$$x(\alpha_1, \alpha_2) = \frac{\alpha_1 + 1}{\alpha_2 - \alpha_1}, \qquad x_a(\beta') = \frac{\beta' - 1}{3 - \beta'}. \tag{A2}$$

Particularly, for a likely case of $\beta' = 5/3$ (reflecting the Kolmogorov turbulence), we have $x_a = 1/2$.

In conjunction with the synchrotron spectrum, in the very high frequency range of $\nu > \nu_c^*$, the F_ν spectrum could have an index of $\alpha_3 = \beta$ (§§ 2.2 and 3.3; eq. [B1]). As is, it may be also instructive to clarify what condition would determine the softening ($\alpha_3 > \alpha_2$) or hardening ($\alpha_3 < \alpha_2$) of the spectrum above ν_c^*. The algebraic manipulations lead to the *Ansatz* that the relation $\beta > \alpha_2$ ($\beta < \alpha_2$) is obtained for the condition $\alpha_2 > \alpha_2^\dagger$ ($\alpha_2 < \alpha_2^\dagger$), where the critical index $\alpha_2^\dagger$ can be expressed as a function of α_1 and β' in the form

$$\alpha_2^\dagger(\alpha_1, \beta') = \frac{x_b(\alpha_1, \beta') + \sqrt{x_b^2(\alpha_1, \beta') - 12\alpha_1 x_a(\beta') x_c(\beta')}}{6x_a(\beta')}, \tag{A3}$$

where the abbreviations are $x_b = \alpha_1(1 + 3x_a) + x_c$ and $x_c = 1 - x_a$. In the special case that satisfies the equality of $\alpha_2 = \alpha_2^\dagger$, we have the relation of $\alpha_2 = \beta$ leading to a common index of $\alpha_3 = \alpha_2$. For example, given $\alpha_1 = 0.67$ (at knot A; Perlman et al. 2001), equation (A3) for $\beta' = 5/3$ provides $\alpha_2^\dagger \simeq 1.3$, whereby the comparison with the index of $\alpha_2 = 1.46 \pm 0.05$ to 1.57 ± 0.10 at the corresponding point (Marshall et al. 2002) leads to $\alpha_3 > \alpha_2$.

B. THE COOLING TIMESCALE AND FLUX DENSITY LEVEL OF THE DIFFUSE SYNCHROTRON RADIATION

On the theoretical basis by Toptygin & Fleishman (1987), we derive the cooling time of the diffuse synchrotron radiation of additionally accelerated electrons in the magnetized filamentary plasma. The emissivity of a single electron by the diffuse synchrotron radiation can be expressed as

$$j(\omega, \gamma) = \frac{2^\beta (\beta - 1)(\beta^2 + 7\beta + 8)}{\beta(\beta + 2)^2(\beta + 3)} \frac{e^2}{c} \frac{\omega_{\rm st}^2}{\omega_0} \left(\frac{\gamma^2 \omega_0}{\omega} \right)^\beta \tag{B1}$$

for ω ($= 2\pi\nu$) $\gg \gamma^2\omega_0$, where $\omega_{\rm st} \equiv eB/(mc)$ and $\omega_0 \equiv 2\pi c/\langle\lambda\rangle$ (Fleishman 2006). In general, the temporal decay of the electron kinetic energy conforms to $-(d\epsilon/dt) = \int d\omega j(\omega, \epsilon)$,

where $\epsilon = \gamma mc^2$ (Longair 1994). For convenience, here we set the lower limit of the ω integral to $\gamma^2\omega_0$ and introduce the variable transformation of $\omega/(\gamma^2\omega_0) = \xi$. Then we have

$$\begin{aligned}\int_{\gamma^2\omega_0}^{\infty} d\omega \frac{\omega_{\rm st}^2}{\omega_0}\left(\frac{\gamma^2\omega_0}{\omega}\right)^{\beta} &= \gamma^2\omega_{\rm st}^2\int_1^{\infty}\xi^{-\beta}d\xi \\ &= \frac{1}{\beta-1}\gamma^2\omega_{\rm st}^2. \end{aligned} \tag{B2}$$

Making use of equation (B2), we obtain the temporal evolution equation of ϵ as follows:

$$-\left(\frac{d\epsilon}{dt}\right) = \frac{4}{3}\tilde{\tau}^{-1}(\beta)\sigma_{\rm T}cu_m\left(\frac{\epsilon}{mc^2}\right)^2, \tag{B3}$$

where $\sigma_{\rm T}$ is the Thomson cross section, $u_m \equiv B^2/8\pi$, and

$$\tilde{\tau}(\beta) \equiv (6\pi)^{-2}\,\frac{\beta\,(\beta+2)^2\,(\beta+3)}{2^{\beta}\,(\beta^2+7\beta+8)}. \tag{B4}$$

The solution of equation (B3) is found to be $\epsilon(t) = \epsilon_0\,(1+t/t_{\rm syn})^{-1}$, where ϵ_0 $(= \gamma_0 mc^2)$ $\equiv \epsilon(t=0)$. Here $t_{\rm syn}$ defines the characteristic decay time for the diffuse synchrotron radiation, which can be expressed as $t_{\rm syn} = \tilde{\tau}\hat{t}_{\rm syn}$, where $\hat{t}_{\rm syn} \equiv 3mc/(4\sigma_{\rm T}u_m\gamma_0)$. Note that the form of $\hat{t}_{\rm syn}$ appears to be the same as that for the normal synchrotron cooling time (Longair 1994), although u_m now includes the rms field strength B, instead of a mean field strength. For values of, e.g., $\beta = 4.3$ and 6.6, equation (B4) gives $\tilde{\tau} = 3.1\times10^{-3}$ and 1.4×10^{-3}, respectively.

In terms of the diffuse synchrotron radiation spectrum of $J_d(\omega) = \int j(\omega,\epsilon)\kappa\epsilon^{-p}d\epsilon$, we pay attention to the ratio to the ordinary synchrotron spectrum [e.g., eq. [18.49] for $J(\omega)$ in Longair 1994]. Particularly, at $\omega_c^* = 2\pi\nu_c^*$ the ratio can be written in the following form:

$$\begin{aligned}\left[\frac{J_d(\omega)}{J(\omega)}\right]_{\omega=\omega_c^*} &= \frac{2^{-p/2}}{27\pi g(p)}\frac{(2/3)^{\beta-(1/2)}\,(\beta-1)}{(2\beta+p+1)\,\tilde{\tau}(\beta)}\left(\frac{\omega_{\rm st}}{\omega_0}\right)^{-(\beta-1)}\left(\frac{\gamma_c}{\gamma_c^*}\right)^{2\beta-p+1} \\ &= \left(\frac{F_{\nu,d}}{F_\nu}\right)_{\nu=\nu_c^*}, \end{aligned} \tag{B5}$$

where the dimensionless function $g(p)$ including gamma functions is identical with the $a(p)$ of equation (18.49) and Table 18.2 in Longair (1994). It is noted that in the derivation of equation (B5), the relation of $\omega_{\rm st}/\omega_c^* = (2/3)(\gamma_c^*)^{-2}$, which is valid for the ordering $B \sim |\mathbf{B}|_{\lambda=\lambda_c}$, has been used. For a value of β that is not small, the factor $(\omega_{\rm st}/\omega_0)^{-(\beta-1)}$ can be considerably small (because typically $\omega_{\rm st}/\omega_0 \gg 1$), such that the flux density ratio, $(F_{\nu,d}/F_\nu)_{\nu=\nu_c^*}$, is much smaller than unity (see eq. [8] for $\beta = 4.3$). By contrast, for a not-so-small value of

equation (B5) that might be realized at inner knots (such as knot D) with a smaller value of $\beta \sim 2-3$ (§ 2.2), the energetic tail of the diffuse synchrotron radiation can appear above ν_c^*, to exhibit $F_{\nu,d} \propto \nu^{-\beta}$.

C. THE BEND-OVER FREQUENCY OF THE VARIATION POWER SPECTRUM FOR BLAZAR GEOMETRY

We check the validity of equation (10) by comparing with the corresponding frequency of the variation power spectrum for blazar jet geometry with a narrow viewing angle. This is associated with (1) application of the filamentary jet model to blazar jets and (2) verification of the idea regarding the FR I radio jet as a misaligned BL Lac object (Tsvetanov et al. 1998); that is, unifying astrophysical jets. If we take the relativistic beaming of the filamentary bulk flow into account, the synchrotron frequency is boosted by the beaming factor δ (i.e., $\nu \propto \delta\gamma^2|\mathbf{B}|$ in the laboratory frame), such that the expression of $\gamma(\lambda,\nu)$ denoted in § 4 should be also corrected, to be multiplied by $\delta^{-1/2}$. Note that the expression of $\gamma_e^*(\lambda)$ (derived from the spatiolimit) is unchanged. For electron acceleration by fully relativistic shocks (with the Lorentz factor Γ), we expect that a strong anisotropy of the momentum distribution function is established, such that the accelerated electrons are preferentially directed in the narrow cone angle of order $\sim 1/\Gamma$ (in the bulk rest frame), regardless of the complexity of turbulent scatterers (Achterberg et al. 2001). This implies that the transverse light-crossing will be delayed by a factor of Γ. Therefore, the bend-over frequency in the laboratory frame may be redefined as $f_b \equiv \delta[c/(\Gamma\lambda_b)]$, where λ_b denotes the solution λ of the equality $\delta^{-1/2}\gamma(\lambda,\nu) = \gamma_e^*(\lambda)$ (see also § 4). As a consequence, we find that f_b can be expressed as

$$f_b = \frac{c\delta}{\tilde{l}D\Gamma}\left[\frac{3}{4\pi}\left(\frac{e}{mc}\right)\frac{\delta B_m}{\nu}\right]^{2/(3\beta+1)}\left(\frac{eB_m\tilde{l}D}{2mc^2}\right)^{4/(3\beta+1)}. \tag{C1}$$

Particularly, setting $\delta = \Gamma = 1$ and $\beta = 4.3$ yields the scaling of equation (10).

For the bulk Lorentz factor of $\lesssim \Gamma$, we have the relation of $\delta \lesssim \Gamma$ for blazar geometry, and then the scaling of equation (C1), e.g., for $\beta = 4.3$, appears to be equation (10) merely multiplied by the factors of δ/Γ ($\lesssim 1$) and $\delta^{2/(3\beta+1)} = \delta^{0.14}$. For the typical blazar parameters of $B_m = 10^{-1}$ G, $\tilde{l}D = 10^{-2}$ pc, and $\delta = 10$, we obtain the value of $f_b \lesssim 5 \times 10^{-5}$ Hz for $\nu = 10^{18}$ Hz (X-ray light curve), which is reasonably consistent with the observational data (e.g., $f_b \simeq 3 \times 10^{-5}$ Hz for Mrk 501; Kataoka et al. 2001). The observational trend of the ν independence of f_b can be also inferred from equation (C1) for conceivable β-values. According to these, the use of equation (10) will be justified for the concerned case of a not-so-

narrow viewing angle and a weak relativistic shock (Biretta et al. 1995; Lobanov et al. 2003).

REFERENCES

Achterberg, A., Gallant, Y. A., Kirk, J. G., & Guthmann, A. W., 2001, MNRAS, 328, 393

Aharonian, F. 2001, in Proc. 27th Int. Cosmic Ray Conf. (Hamburg), 250

Aharonian, F., et al. 2003, A&A, 403, L1

Bai, J. M., & Lee, M. G. 2001, ApJ, 549, L173

Beilicke, M., et al. 2005, in Proc. 29th Int. Cosmic Ray Conf. (Pune), 4, 299

Biermann, P. L., & Strittmatter, P. A. 1987, ApJ, 322, 643

Biretta, J. A., Stern, C. P., & Harris, D. E. 1991, AJ, 101, 1632

Biretta, J. A., Zhou, F., & Owen, F. N. 1995, ApJ, 447, 582

Capetti, A., Macchetto, F. D., Sparks, W. B., & Biretta, J. A. 1997, A&A, 317, 637

Carilli, C. L., & Barthel, P. D. 1996, A&A Rev., 7, 1

Coppi, P. S., & Aharonian, F. A. 1997, ApJ, 487, L9

Di Matteo, T., Allen, S. W., Fabian, A. C., Wilson, A. S., & Young, A. J. 2003, ApJ, 582, 133

Fleishman, G. D. 2006, MNRAS, 365, L11

Gould, R. J., & Schréder, G. 1966, Phys. Rev. Lett., 16, 252

Heinz, S., & Begelman, M. C. 1997, ApJ, 490, 653

Hofmann, W. 2001, in Proc. 27th Int. CosmicvRay Conf. (Hamburg), 2785

Honda, M., & Honda, Y. S. 2002, ApJ, 569, L39

——. 2004a, ApJ, 617, L37

——. 2005a, ApJ, 633, 733

Honda, M., Meyer-ter-Vehn, J., & Pukhov, A. 2000a, Phys. Plasmas, 7, 1302

——. 2000b, Phys. Rev. Lett., 85, 2128

Honda, Y. S., & Honda, M. 2004b, ApJ, 613, L25

——. 2005b, MNRAS, 362, 833

Jokipii, J. R. 1987, ApJ, 313, 842

Kardashev, N. S. 1962, Soviet Astron.–AJ, 6, 317

Kataoka, J., et al. 2001, ApJ, 560, 659

Keel, W. C. 1988, ApJ, 329, 532

Kneiske, T. M., Bretz, T., Mannheim, K., & Hartmann, D. H. 2004, A&A, 413, 807

Kneiske, T. M., & Mannheim, K. 2005, Proc. 29th Int. Cosmic-Ray Conf. (Pune), 4, 1

Le Bohec, S., et al. 2004, ApJ, 610, 156

Lobanov, A., Hardee, P., & Eilek, J. 2003, New A Rev., 47, 629

Longair, M. S. 1992, High Energy Astrophysics, Vol. 1: Particles, Photons and Their Detection (Cambridge: Cambridge Univ. Press)

——. 1994, High Energy Astrophysics, Vol. 2: Stars, the Galaxy and the Interstellar Medium (Cambridge: Cambridge Univ. Press)

Marshall, H. L., Miller, B. P., Davis, D. S., Perlman, E. S., Wise, M., Canizares, C. R., & Harris, D. E. 2002, ApJ, 564, 683

McEnery, J. E., Moskalenko, I. V., & Ormes, J. F. 2004, in Cosmic Gamma-Ray Sources, ed. K. S. Cheng & G. E. Romero (Dordrecht; Kluwer), 361

Meisenheimer, K., Röser, H.-J., & Schlötelburg, M. 1996, A&A, 307, 61

Montgomery, D., & Liu, C. S. 1979, Phys. Fluids, 22, 866

Nikishov, A. I. 1962, Sov. Phys.–JETP, 14, 393

Ostrowski, M. 2000, MNRAS, 312, 579

Owen, F. N., Eilek, J. A., & Keel, W. C. 1990, ApJ, 362, 449

Owen, F. N., Hardee, P. E., & Cornwell, T. J. 1989, ApJ, 340, 698

Pérez-Fournon, I., Colina, L., González-Serrano, J. I., & Biermann, P. L. 1988, ApJ, 329, L81

Perlman, E. S., Biretta, J. A., Sparks, W. B., Macchetto, F. D., & Leahy, J. P. 2001, ApJ, 551, 206

Perlman, E. S., Biretta, J. A., Zhou, F., Sparks, W. B., & Macchetto, F. D. 1999, AJ, 117, 2185

Perlman, E. S., & Wilson, A. S. 2005, ApJ, 627, 140

Protheroe, R. J., Donea, A.-C., & Reimer, A. 2003, Astropart. Phys., 19, 559

Protheroe, R. J., & Meyer, H. 2000, Phys. Lett. B, 493, 1

Reid, M. J., Biretta, J. A., Junor, W., Muxlow, T. W. B, & Spencer, R. E. 1989, ApJ, 336, 112

Reimer, A., Protheroe, R. J., & Donea, A. C. 2004, A&A, 419, 89

Reimer, O., Pohl, M., Sreekumar, P., & Mattox, J. R. 2003, ApJ, 588, 155

Schlickeiser, R. 2002, Cosmic Ray Astrophysics (Berlin: Springer)

Silva, L. O., Fonseca, R. A., Tonge, J. W., Dawson, J. M., Mori, W. B., & Medvedev, M. V. 2003, ApJ, 596, L121

Sreekumar, P., et al. 1998, ApJ, 494, 523

Stawarz, Ł., Aharonian, F., Kataoka, J., Ostrowski, M., Siemiginowska, A., & Sikora, M. 2006a, MNRAS, 370, 981

Stawarz, Ł., Kneiske, T. M., & Kataoka, J. 2006b, ApJ, 637, 693

Stawarz, Ł., Sikora, M., & Ostrowski, M. 2003, ApJ, 597, 186

Stiavelli, M., Møller, P., & Zeilinger, W. W. 1991, Nature, 354, 132

Stiavelli, M., Peletier, R. F., & Carollo, C. M. 1997, MNRAS, 285, 181

Strong, A. W., Moskalenko, I. V., & Reimer, O. 2004, ApJ, 613, 956

Takahashi, T., et al. 2004, Proc. SPIE, 5488, 549

Tonry, J. L. 1991, ApJ, 373, L1

Toptygin, I. N., & Fleishman, G. D. 1987, Ap&SS, 132, 213

Tsvetanov, Z. I., Hartig, G. F., Ford, H. C., Dopita, M. A., Kriss, G. A., Pei, Y. C., Dressel, L. L., & Harms, R. J. 1998, ApJ, 493, L83

Vainio, R. 1999, in Plasma Turbulence and Energetic Particles in Astrophysics, ed. M. Ostrowski & R. Schlickeiser (Kraków: Obs. Astron.), 232

Wei, M. S., et al. 2004, Phys. Rev. E, 70, 056412

Wilson, A. S., & Yang, Y. 2002, ApJ, 568, 133

This preprint was prepared with the AAS LaTeX macros v5.2.

FIGURE CAPTIONS

Fig. 1.— Lorentz factor of an electron achievable for a conventional DSA γ^*, vs. the transverse size of a magnetized filament λ for a fixed b and some given values of B_m (*as labeled*; *top*) and vice versa (*middle*), and for $b = 10^{-3}$ and $B_m = 4.59$ mG (*bottom*; Owen et al. 1989), indicating the regimes where γ^* is determined by the spatial (*thick dotted line*) and temporal limits (synchrotron loss; *thick solid curve*). Here b is the energy density ratio of the Alfvénic fluctuation/local mean magnetic field, B_m is the magnetic intensity of the filament with λ reaching a correlation length compared to the jet diameter, $D = 110$ pc at knot A (*thin long-dashed line*; Biretta et al. 1991), and more on the DSA parameters (at the knot A region) is given in the text. The axes are common in the figures. Note that the solid curve in the top panel is the same as that in the middle panel. In the bottom panel, the thin dot-dashed curve indicates the (pseudo)limit due to the Thomson scattering, which is removed by the Klein-Nishina effect, and the accelerator is active in the shaded domain, wherein the solid arrows represent the pre-DSA of the electrons bound to the filaments with $\lambda < \lambda_c$, leading to the escape (bound-free transition) entailed in the injection of additional DSA, and the dotted arrows represent the energization that is knocked down by the synchrotron loss before the escape, namely, the tracks of secular traps in the filaments with $\lambda > \lambda_c$. [*See the electronic edition of the Journal for a color version of this figure.*]

Fig. 2.— Dependencies of the break ν_b (*top*), the critical frequency ν_c^* (*middle*), and the flux density reduction factor ϕ (defined in eq. [2]; *bottom*) on B_m, for $b = 10^{-4} - 10^{-2}$ (*as labeled*) and the correlation length of filaments compared to D (= 110 pc; *thick curves*) and $0.1D$ (*thin curves*). Here the other DSA parameters are the same as those for Fig. 1. The horizontal axis is common in the figures. Note that in the middle panel, the thick solid and dot-dashed lines overlap the thin ones, and in the bottom panel, the thick dot-dashed line overlaps the thin dotted line.

Fig. 3.— Transitive synchrotron spectral index α_2 (eq. [3]) vs. the power-law spectral index of filamentary turbulence β for the given canonical index α_1 as a parameter (*as labeled*). In connection with observed synchrotron spectra, α_1 and α_2 can be typically compared to the radio-optical and X-ray spectral indices, respectively. For further explanation, see the text.

Fig. 4.— Cutoff Lorentz factor of an additionally accelerated electron γ_c vs. the target photon frequency ν_t, for the energy density ratio of target photons/magnetic fields in the range $a = 10^1 - 10^6$ (*as labeled*). Here the parameters relevant to shock and filamentary turbulence are the same as those for Fig. 1 (see also the text). The dotted line indicates $\epsilon = \gamma_c h\nu_t/(mc^2) = 1$: the region of $\epsilon \ll 1$ reflects the Thomson limit, in which the values of γ_c take constants, while $\epsilon \gtrsim 1$ indicates the Klein-Nishina regime. An asymptotic value for

$a\tilde{\tau} \ll 1$ ($\tilde{\tau} \simeq 3 \times 10^{-3}$) provides the upper bound of γ_c (independent of the rms magnetic field strength B), which is referred to as the diffuse synchrotron limit.

Fig. 5.— Cutoff frequency of the inverse Compton gamma-ray radiation $\nu_{\mathrm{ic},c}$ vs. the target photon frequency ν_t for $a = 10^1 - 10^6$ (*as labeled*), corresponding to the cases shown in Fig. 4. The ranges of characteristic frequency for the candidate external Compton (EC) sources of the starlight ("Star"), dust emission ("Dust"), and the cosmic microwave background ("CMB") are also indicated for the bulk Lorentz factor of $1 - 10$ (*arrows*; Stawarz et al. 2003).

Fig. 6.— Model νF_ν spectrum of synchrotron radiation for $\beta = 4.3$ (*solid curve*) and 6.6 (*dotted curve*), and for the former, the source spectrum of IC radiation for the possible cases of $a = 10^{-1}$ (*dashed curve*) and 10^{-2} (*dot-dashed curve*) in the knot A environment. Here the EC target photon frequency has been supposed to be $\nu_t = 10^{14}$ Hz, and the other conditions are the same as those for Figs. 1 (*bottom*) and 4. The open squares and diamond indicate the data measured in the near-infrared to optical (Perlman et al. 2001) and X-ray (Marshall et al. 2002) bands, respectively, and the open and filled triangles indicate the gamma-ray levels detected by HEGRA (Aharonian et al. 2003) and HESS (Beilicke et al. 2005), respectively. In addition, the EGRET (Reimer et al. 2003) and Whipple 10 m telescope (Le Bohec et al. 2004) upper limits are indicated. For convenience, the sensitivity limits of a currently operating Cerenkov telescope (HESS; Hofmann 2001) and future detectors (*GLAST* LAT, McEnery et al. 2004; *New X-Ray Telescope* Hard X-Ray Imager and Soft Gamma-Ray Detector [*NeXT* HXI and SGD], Takahashi et al. 2004) are also depicted. The intrinsic cutoff and expected range of the observed cutoff as a result of the absorption in the CIB (Coppi & Aharonian 1997; Protheroe & Meyer 2000; Aharonian 2001) are indicated by the thick arrow and the thick bar with thin dotted lines, respectively. Note that the diffuse synchrotron component that appears in the high-energy gamma-ray region is of a considerably lower level. [*See the electronic edition of the Journal for a color version of this figure.*]

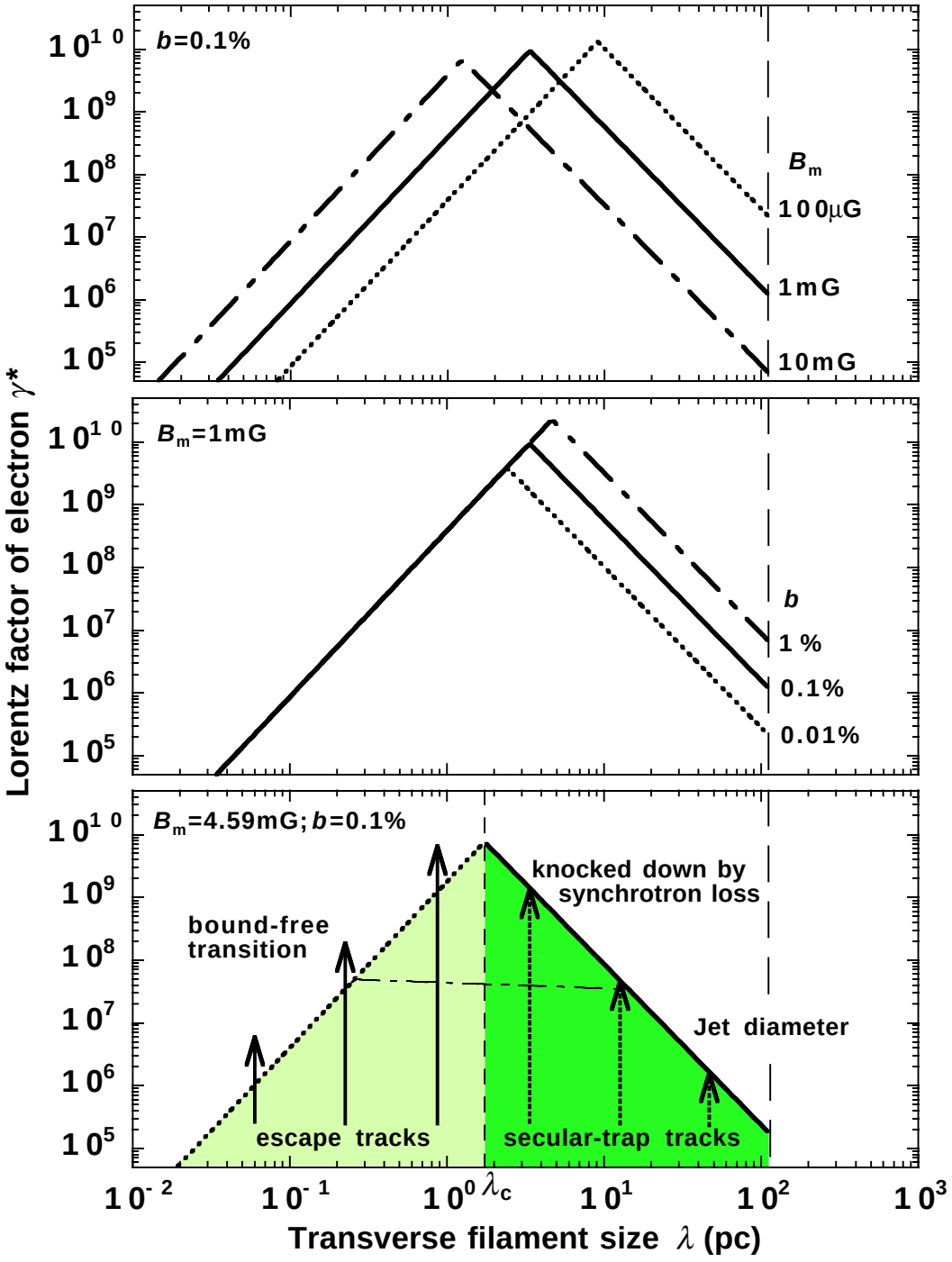
b=0.1%
B_m
100μG
1mG
10mG
B_m=1mG
b
1 %
0.1%
0.01%
B_m=4.59mG; b=0.1%
knocked down by
synchrotron loss
bound-free
transition
Jet diameter
escape tracks
secular-trap tracks
Lorentz factor of electron γ*
Transverse filament size λ (pc)
λc

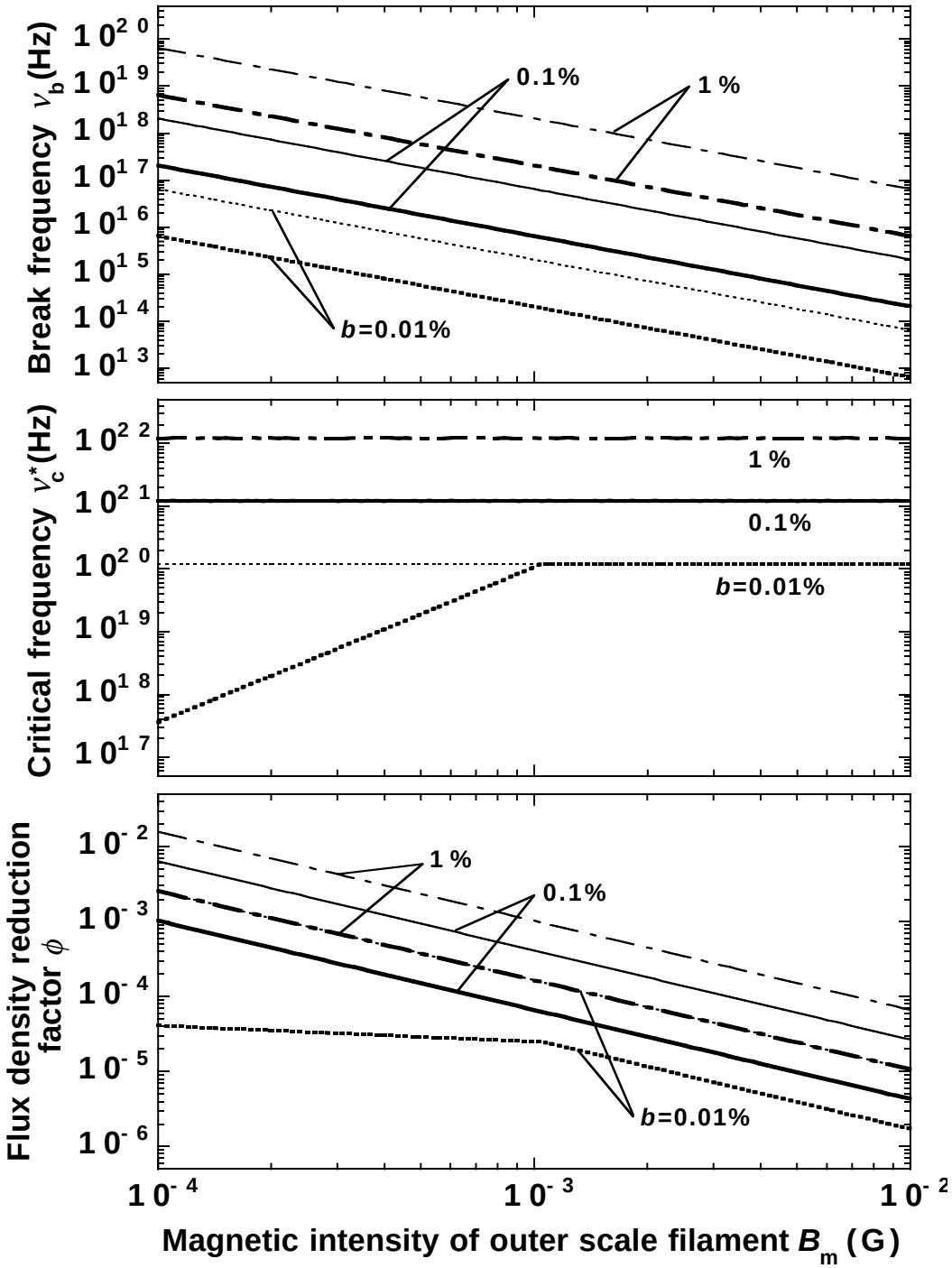
Break frequency ν_b(Hz)
10^{20}
10^{19}
10^{18}
10^{17}
10^{16}
10^{15}
10^{14}
10^{13}
0.1%
1 %
b=0.01%
Critical frequency ν_c^*(Hz)
10^{22}
10^{21}
10^{20}
10^{19}
10^{18}
10^{17}
1 %
0.1%
b=0.01%
Flux density reduction factor ϕ
10^{-2}
10^{-3}
10^{-4}
10^{-5}
10^{-6}
1 %
0.1%
b=0.01%
10^{-4}
10^{-3}
10^{-2}
Magnetic intensity of outer scale filament B_m (G)

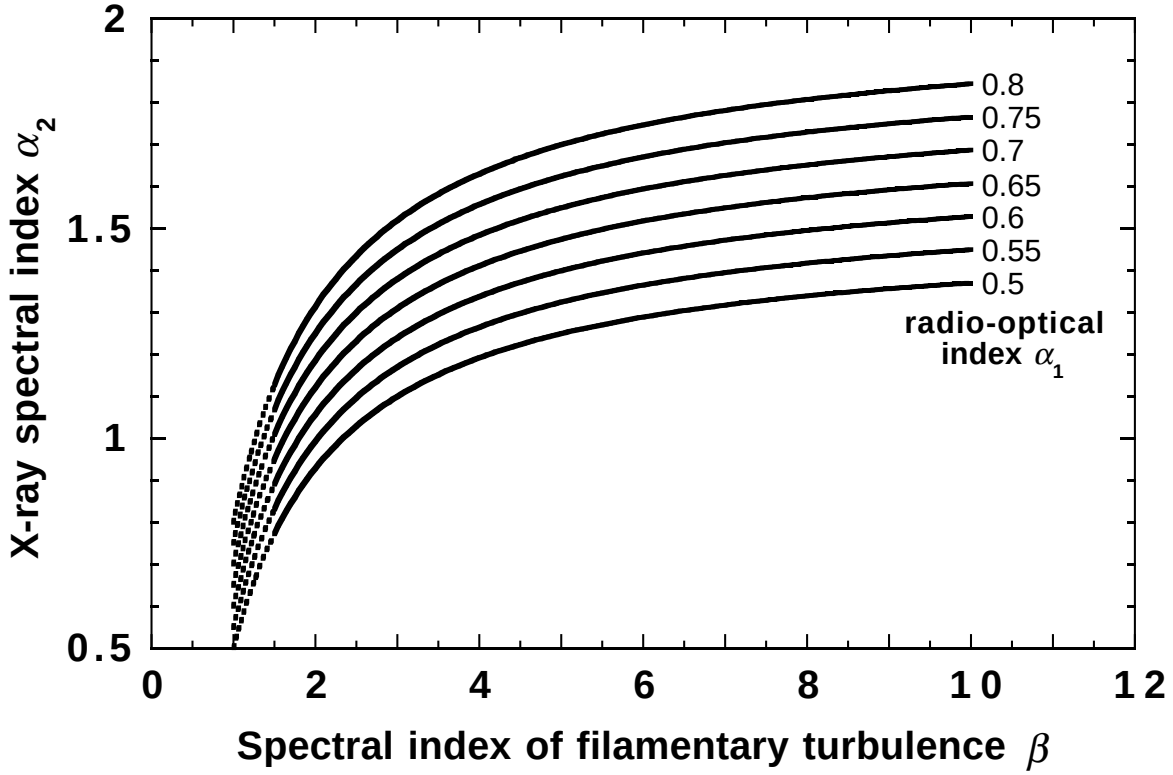
2
1.5
1
0.5
0
2
4
6
8
10
12
X-ray spectral index α_2
Spectral index of filamentary turbulence β
0.8
0.75
0.7
0.65
0.6
0.55
0.5
radio-optical
index α_1

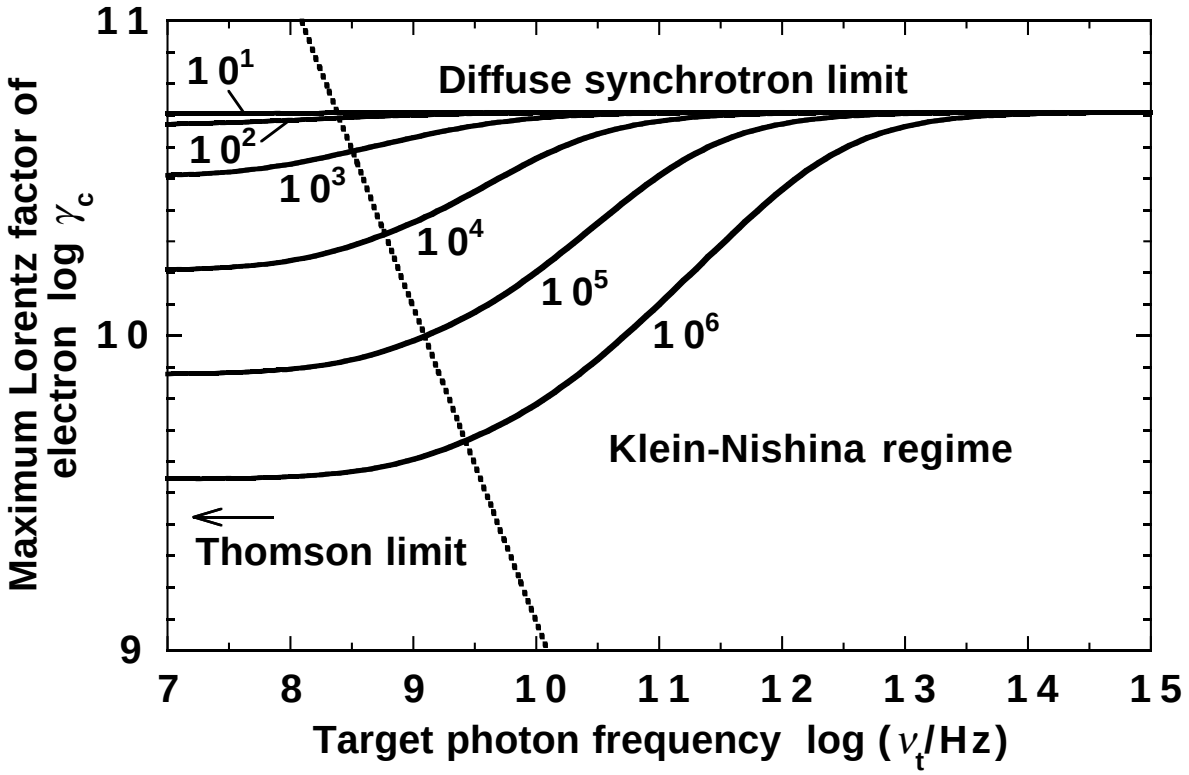
11
10
9
7
8
9
10
11
12
13
14
15
Maximum Lorentz factor of electron log γ_c
Target photon frequency log (ν_t/Hz)
10^1
10^2
10^3
10^4
10^5
10^6
Diffuse synchrotron limit
Klein-Nishina regime
Thomson limit

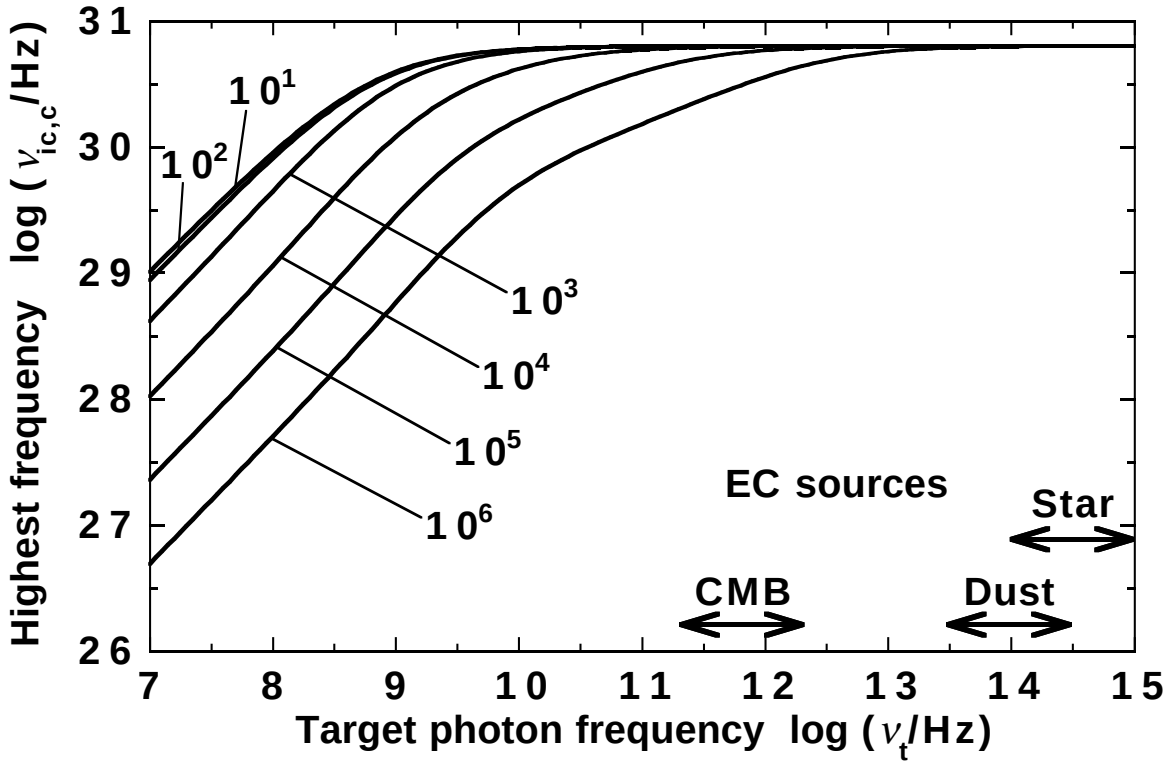
Highest frequency log ($\nu_{ic,c}$ /Hz)
Target photon frequency log (ν_t/Hz)
10^1
10^2
10^3
10^4
10^5
10^6
EC sources
Star
CMB
Dust
31
30
29
28
27
26
7
8
9
10
11
12
13
14
15

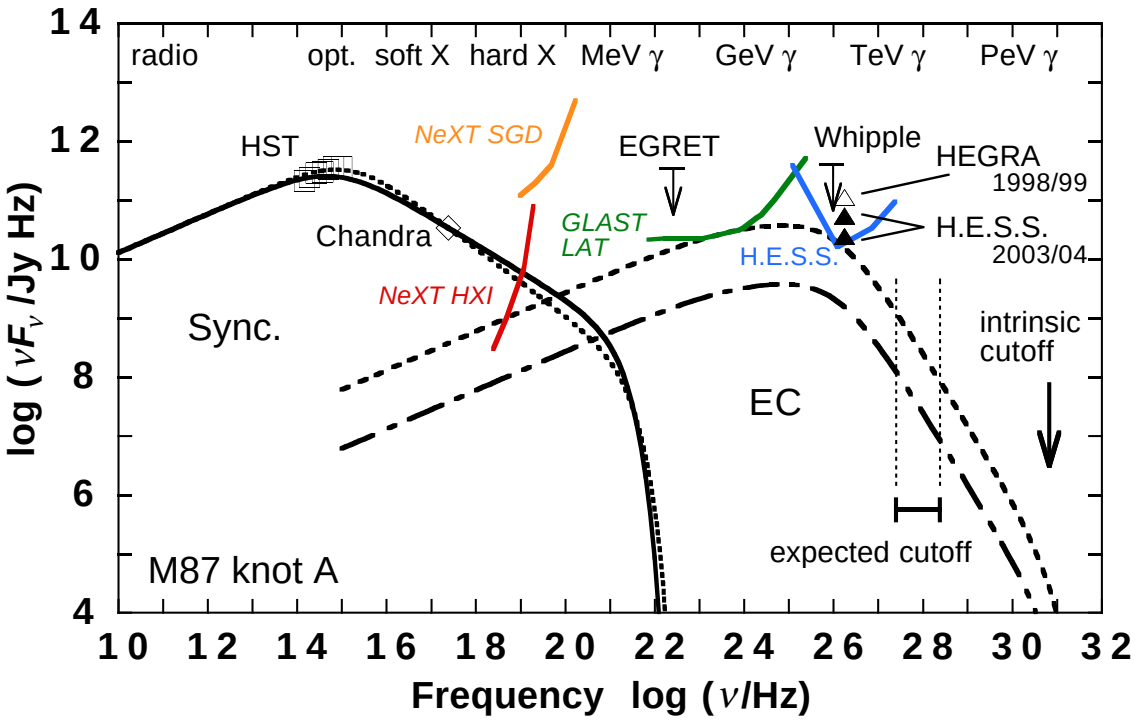
radio
opt.
soft X
hard X
MeV γ
GeV γ
TeV γ
PeV γ
HST
NeXT SGD
EGRET
Whipple
HEGRA
1998/99
Chandra
GLAST
LAT
H.E.S.S.
2003/04
H.E.S.S.
NeXT HXI
Sync.
intrinsic
cutoff
EC
expected cutoff
M87 knot A
log (νF_ν /Jy Hz)
Frequency log (ν/Hz)
14
12
10
8
6
4
10
12
14
16
18
20
22
24
26
28
30
32